Theoretical principles of holographic crystallography

D. K. Saldin, G. R. Harp, B. L. Chen, and B. P. Tonner
Department of Physics, University of Wisconsin-Milwaukee, 1900 East Kenwood Boulevard, Milwaukee, Wisconsin 53211
(Received 28 January 1991)

We examine the theory of electron holography with atomic electron sources and its potential for local crystallography. We simulate electron diffraction pattern by full multiple-scattering cluster calculations and examine the nature of the reconstructed images. We draw attention to the power of the zone-plate model of holography for understanding the results, and in particular to the optimal reconstructing properties of the Gabor zone plate, which in turn suggests the form of an optimal reconstruction algorithm.

I. INTRODUCTION

Considerable excitement has been generated recently by the infusion of holographic ideas[1-3] for the interpretation of diffuse electron diffraction patterns of various kinds. The prospect has arisen of dispensing with the need for the time-consuming trial-and-error fitting of calculated diffraction patterns to experimentally measured ones for the extraction of atomic structural information. It has been suggested that the principle of holographic reconstruction[4] may form the basis of an elegant *direct* method of structure determination. Accordingly we term the technique "holographic crystallography." The first experimental demonstration of such ideas was reported recently by us in the cases of reflection Kikuchi patterns[5] and Auger emission patterns[6] from Cu(100) and Cu(111) surfaces. Similar results were subsequently obtained by Wei, Zhao, and Tong[7,8] from calculated photoelectron diffraction patterns from Co/Cu(111) and hcp Co(0001) surfaces, respectively.

In the holographic interpretation of such diffraction patterns, reference waves are generated in the vicinity of individual atoms, and object waves arise from the scattering of this radiation by other atoms close to the reference wave sources. Fraunhofer holograms are formed and recorded in the far field in the form of a diffuse diffraction pattern. In many respects, however, atoms are quite unlike the objects whose images are formed in conventional optical holography. Atoms are not merely amplitude-reflecting objects for electrons—they also affect the phases of the scattered waves and, for electron energies greater than about 500 eV, are highly nonisotropic scatterers. These facts have profound implications for the forms of the reconstructed atomic images. In the "forward-scattering" geometry the scattering objects are found close to the direct path between the source and the detector, and the form of the diffraction pattern is greatly influenced by the strongly forward-peaked nature of the atomic scattering factors for electrons of medium energy ($\sim$1000 eV) and is little affected by atomic back-scattering processes. In order to perform the holographic reconstruction step by computer, Barton[2] proposed a Fourier transform algorithm based on the Helmholtz-Kirchhoff integral. When such an algorithm is used for forward-scattering diffraction patterns we found[5,6] that the images of atoms appear ellipsoidal, with their major axes oriented along the forward-scattering direction.[5,6] The appearance of forward-scattering diffraction patterns is often dominated by features (the forward-scattering peaks) arising from the forward-peaked nature of the atomic scattering factors, but the holographic information resides in diffraction fringes, which are spread over large areas of the diffraction pattern. The forward-scattering peaks themselves, so useful in the identification of the directions of atomic chains, turn out to be the cause of identifiable interatomic artifacts on reconstructed images.[9]

When single scattering dominates in the forward-scattering geometry, as in the case of photoelectron diffraction due to electrons emitted from an atom in a molecule adsorbed on a surface, or from atoms in an ultrathin film, the phase and amplitude variations of the atomic scattering factors cause the atom images to be shifted further away from the emitter atom than the true positions of the scattering atoms. In order to correct for such atom shifts, and to improve the resolution of the atomic images, more sophisticated reconstruction algorithms have been suggested by Tong *et al.*[10] and by ourselves.[11] Both these schemes seek to correct the holograms for the angular variation of the phases and amplitudes of the atomic scattering factors. We present here a critical comparison of the two schemes. When multiple-scattering acts so as to reduce the dominance of the forward-scattering peaks, the Helmholtz-Kirchhoff scheme[2] is found to be adequate.

In contrast to the forward-scattering geometry discussed above, we refer to a configuration in which the scattering objects are further from the measured diffraction pattern than the source, as the "back-scattering geometry." An example of such a geometry is that in which an adsorbate atom on a surface is a source of electrons. The resulting diffraction pattern is dominated by the interference between the direct wave from the source and *back-scattered* waves from its nearby substrate atoms. Although the small momentum transfer associated with forward-scattering events results in temperature having relatively little influence on diffraction patterns from such a geometry, "back-scattering" diffraction pat-

terns are greatly affected by the sample's temperature due to the greater effect of the Debye-Waller factor for high-momentum transfers. Thus we find that although signal-to-noise problems may seriously hinder the measurement of holographic fringes on back-scattering patterns due to medium-energy electrons at room temperature, such measurements may become very feasible near liquid-nitrogen temperatures. Although the back-scattering part of atomic scattering factors of electrons of such energies show much less angular variation, our new reconstruction algorithm[11] is found to improve the accuracy of the determination of the atom centers in the back-scattering geometry also.

The work presented here is essentially theoretical, although comparisons with experimental results is made where appropriate. Diffraction patterns are calculated by a full multiple-scattering cluster scheme,[12] developed originally for low-energy electron diffraction (LEED). The lack of any assumption of long-range order enables us to examine the effects of the presence or absence of individual atoms or groups of atoms, allowing an isolation of the effects of particular scattering paths. We find that considerable insight into the nature of the holographic processes may be gained by an analysis of very small atomic clusters.

II. THE CALCULATION OF THE DIFFRACTION PATTERNS

The form of a diffraction pattern due to the emission of electrons from atomic sources is determined largely by the interference between the directly emitted electrons and those scattered by nearby atoms. Since the latter electrons may be multiply scattered by many of the nearby atoms, an adequate theory needs to take this into account. An approach to the calculation angle-resolved photoemission intensities from an adsorbate on a surface has been suggested by Liebsch.[13] The theory was extended by Davis and Kaplan[14] and by Tong and coworkers[15,16] for core-level photoemission from substrate atoms, with the multiple scattering of the emitted electrons evaluated by calculating the scattering properties of atomic layers parallel to a crystal surface, as in conventional theories of LEED.[17] A different approach has been taken by Barton and Shirley[18] and by Fritzsche[19] in which the near neighbors of the emitter are regarded as a cluster of atoms, thus overcoming the restriction of long-range two-dimensional order. In order to make the calculations tractable, Barton and Shirley used the Taylor-series magnetic-quantum-number expansion (TS-MQNE), and Fritzsche the reduced-angular-momentum expansion (RAME), both approximation schemes that restrict the number of angular-momentum components of appropriately rotated interatom electron propagators. Recently Kaduwela, Friedman, and Fadley[20] have reported the development of a similar computational scheme, which takes account of a finite number of scattering events and where the propagators took the form of the so-called separable Green functions of Rehr and Albers.[21]

In this paper we report the use of an *exact* multiple-scattering scheme for the calculation of electron diffraction from a cluster surrounding an atom emitter, in which the multiple-scattering paths are summed to infinity. Our method is based on a division of the cluster into a series of shells, and where the scattering paths are classified as intrashell or intershell processes. Due to the fact that, for medium-energy electrons in this geometry, intershell scattering is likely to be much more significant than its intrashell counterpart, such a decomposition of multiple-scattering paths forms the basis of a practical alternative computational scheme. Our method is somewhat similar to one employed for the calculation of x-ray-absorption near-edge structure (XANES);[22,23] and, even more so, to a scheme developed by Pendry and Saldin for LEED.[24,12] A fuller account of our theory will be given in a subsequent article. In this paper we consider only the scattering from a single shell of atoms surrounding the emitter, when the theory takes on a particularly simple form.

On a muffin-tin model, we can, in general, write the wave function of monochromatic electrons emitted from an atom as

$$\psi(\mathbf{r})=\sum_{l,m} A_{lm} h_l^{(1)}(kr) Y_{lm}(\hat{\mathbf{r}}) , \tag{1}$$

where l is the angular momentum and m the magnetic quantum number, $h_l^{(1)}$ a Hankel function, Y_{lm} a spherical harmonic, k the wave number of the electrons, and $\mathbf{r}$ a position vector. After multiple scattering with the shell of atoms surrounding the emitter, the outgoing wave function may be written in the form

$$\psi'(\mathbf{r})=\sum_{l',m'} B_{l'm'} h_{l'}^{(1)}(kr) Y_{l'm'}(\hat{\mathbf{r}}) , \tag{2}$$

where

$$\underline{B}=\underline{A}(\underline{1}-\underline{T}_{\mathrm{OI}}\underline{t})^{-1}\underline{T}_{\mathrm{OO}} . \tag{3}$$

In the above expressions, $\underline{A}$ and $\underline{B}$ are row vectors formed from the elements A_{lm} and B_{lm}, respectively; $\underline{T}_{\mathrm{OO}}$, and $\underline{T}_{\mathrm{OI}}$ are the "out-out" and "out-in" scattering matrices[22] of the shell of atoms surrounding the emitter, and $\underline{t}$ is the diagonal t matrix of the emitter atom, whose nonzero elements are given by

$$t_l=\tfrac{1}{2}(e^{2i\delta_l}-1) , \tag{4}$$

where δ_l is the phase shift of the emitter atom of angular momentum l. Note that equation (3) also takes account of the subsequent scattering of the emitted electron by the emitter atom.

With the asymptotic expansion of the Hankel functions,

$$\lim_{z\to\infty} h_l^{(1)}(z)=(-i)^{l+1}z^{-1}e^{iz} , \tag{5}$$

the diffraction amplitude in the far field may be written as

$$\psi'(\hat{\mathbf{k}})\propto\sum_{l',m'} B_{l',m'}(-i)^{l'}Y_{l',m'}(\hat{\mathbf{k}}) , \tag{6}$$

where $\mathbf{k}$ is the local wave vector of the detected electron.

Since our aim is to analyze the holographic properties of forward-scattering (or "forward-focusing"[25–27]

diffraction patterns, in this paper we consider only the simplest type of emission source, namely, an s-wave emitter, i.e., we take $A_{lm}=\delta_{l0}\delta_{m0}$, and, with the exceptions of Figs. 1(a) and 5, all the emitters and scatterers are assumed to be copper atoms. Generalization to nonisotropic emitters is straightforward, and will be considered in a later publication. The angular-momentum expansions of the atomic-scattering processes take into account quantum numbers up to $l=15$, and the single-center expansions about the central atom are extended up to $l'=50$. The calculations were tested for convergence with respect to these parameters. The zero-temperature phase shifts are corrected for finite temperatures by a Debye-Waller factor[17] assuming a Debye temperature of 320 K and a sample temperature of 300 K, in all cases except that of Fig. 12(b), which assumes a sample temperature of 100 K. For all the atomic clusters, we take into account the full multiple scattering of the electrons between the source and all the scattering atoms. The diffraction patterns are collected over polar angles ranging from 0° to 70°. All the calculations assume an electron kinetic energy (outside the sample) of 914 eV, which is the energy of Cu LVV Auger emission, and an inner potential with real and imaginary parts of -15 and -4 eV, respectively.

III. THE GABOR ZONE PLATE AND THE ATOMIC ZONE PLATE

Our atomic holograms are, as we suggested in our introduction, of a rather unusual kind. We can understand their properties better by comparing them with an optical analogy. Consider a point source of light, which acts as a reference wave, incident on a small reflecting object, which we regard as an isotropic scatterer with a complex scattering factor $f=|f|\exp(i\delta)$, which generates an object wave. The interference pattern on a portion of a spherical screen placed a great distance from the source and scatterer will be symmetric about the axis joining source and scatterer (which we term the principal axis). Its intensity variation thus depends only on the polar angle about this axis, and is represented by

$$H(\theta)=1+|f|^2/r_0^2 +2|f|\cos[kr_0(1-\cos\theta)+\delta]/r_0 , \quad (7)$$

where r_0 is the distance form the source to the scattering object and θ is a polar angle measuring from the line joining the source and scatterer. The argument of the cosine term arises from the path difference between the waves forming the interference pattern. The appearance of such a pattern, projected on a plane perpendicular to the principal axis is shown in Fig. 1(a). For the purposes of the simulation we have taken the wave number, $k=8.2$ (a.u.)$^{-1}$, $r_0=4.82$ a.u. ($=2.55$ Å) for comparison with a realistic simulation, which follows. For simplicity we have taken $|f|/r_0=1$ and $\delta=0$. Figure 1(a) shows all the characteristics of an object well-known in optics, namely, a zone plate, whose properties appear to have been first noted by Rayleigh.[28] Perhaps its best-known form is the Fresnel zone plate, capable of being created by ruling a series of concentric opaque fringes of specified radii on an otherwise transparent material. A beam of light, symmetric about the principal axis, incident on such an object is capable of being brought to a series of foci along the principal axis. The higher-order foci are due to the need for several orders of Fourier coefficients to describe the abrupt intensity variations of the Fresnel zone plate.[29] In this sense, the zone plate described by (7) is unique, in that it is representable by just two Fourier coefficients, from the decomposition of the cosine term in (7) into its exponential components. Such an object is known as a sinusoidal[29] or Gabor[30] zone plate because its relation to holography. Indeed, the so-called zone-plate model of optical holography[29,30] regards a hologram of an extended object as being a superposition of individual Gabor zone plates due to reflected light from each point on that object. On reconstruction, each zone plate reconstructs its corresponding object point, thus faithfully recreating

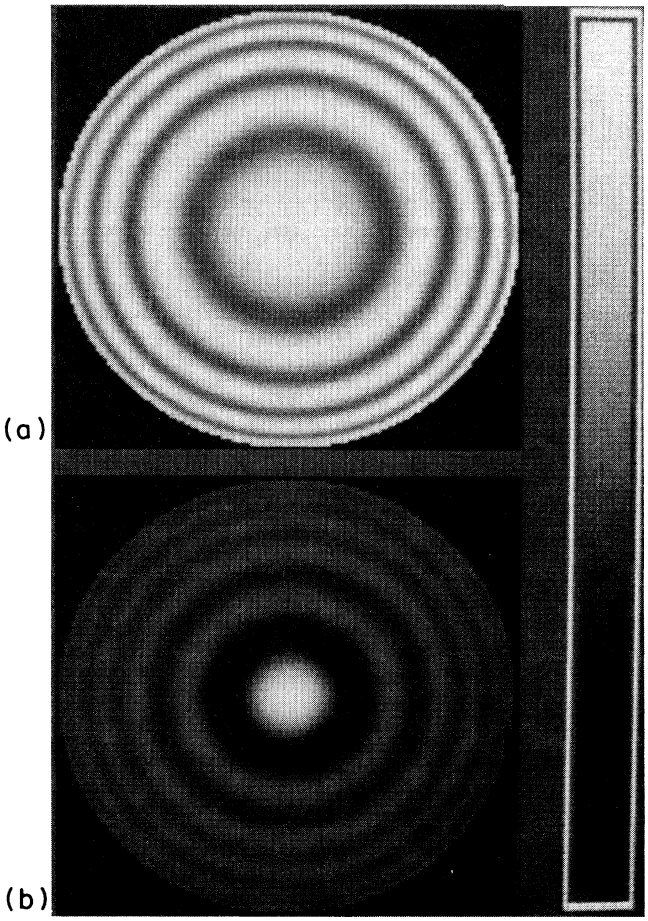

FIG. 1. (a) A Gabor zone plate, the forward-scattering Fraunhofer diffraction pattern generated by a point source of 914-eV electrons and an isotropic scatterer of zero phase shift 2.55 Å from the source. (b) An "atomic" zone plate from the same configuration as (a) but with the isotropic scatterer replaced by a Cu atom. In (b) a very prominent forward-scattering peak is observed with an extra fringe in the diffraction pattern.

the appearance of the extended object.

Thus, the diffraction pattern of Fig. 1(a) may be thought of as the simplest conceivable hologram, and one with ideal reconstruction properties. If a spherical wave of the same wavelength as that used to generate the diffraction pattern and convergent on the original radiation source were incident from the convex side of our hologram, it is brought to two foci in addition to its original point of convergence. One of these will be the true position of the original scattering object, and the other the position of the twin image, equidistant from the source on the other side of the principal axis. The sizes of these foci will be determined by just the diffraction limit, from Abbe's theory of image resolution.[31] All these points are well illustrated by noting that the amplitude of the reconstructed image along the principal axis may be found by rexpressing the Helmholtz-Kirchoff reconstruction algorithm:[2]

$$A(\mathbf{r})=\int H(\hat{\mathbf{k}})\exp(-i\mathbf{k}\cdot\mathbf{r})d\hat{\mathbf{k}} \tag{8}$$

in spherical polars with the polar axis taken along the principal axis. The resulting expression is

$$A(z)=-2\pi\int H(\theta)\exp(-ikz\cos\theta)d(\cos\theta)\ , \tag{9}$$

which is the form of a *one-dimensional* Fourier transform. The integral (9) may be performed analytically for a diffraction pattern of the form (7),[9] and we find that the reconstructed intensity $I(z)=|A(z)|^2$ takes the form

$$I(z)\propto(1-c_m)^2([1+(f/z_0)^2][\sin(\kappa z/2)/(\kappa z/2)]^2+(f/z_0)\{\sin[\kappa(z-z_0)/2]/[\kappa(z-z_0)/2]\}^2 +(f/z_0)\{\sin[\kappa(z+z_0)/2]/[\kappa(z+z_0/2)]\}^2)\ , \tag{10}$$

where

$$\kappa=(1-c_m)k \tag{11}$$

and $c_m=\cos\theta_{\max}$, where $\theta_{\max}$ is the maximum polar angle of the recorded hologram.

Thus we see that the intensity distribution along the principal axis consists of three peaked sinc functions centered on $z=0$ and $\pm z_0$. The first represents the focus of the undiffracted spherical wave, the second the holographic reconstruction of the scattering object, and the third that of the twin image. Since the amplitude terms giving rise to each of the sinc functions above are localized around different regions of the principal axis, we have neglected the small terms due to their mutual interference. Note that the phase shift, δ, of our point scatterer does not appear in (10), indicating that there exists a whole family of Gabor zone plates, corresponding to different values of δ with identical holographic reconstruction properties. If, as is customary, the normalized function $\chi=(H-H_0)/H_0$ (where H_0 is the mean value of H) replaces H in (9), was the case for the function $I(z)$ shown in Fig. 3(a), which was numerically computed for the diffraction pattern of Fig. 1(a), the peak at $z=0$ is eliminated. The width, Δz, of the central peak of each of the sinc functions in (10) is given by

$$\Delta z=2\pi/\kappa\ , \tag{12}$$

which for the assumed values of $k=8.2$ (a.u.)$^{-1}$ and $\theta_{\max}=70°$ is 1.2 Å, in good agreement with that observed in Fig. 3(a). Note that κ is equal to the range Δk, of the values of the z component of the electron wave vector associated with the hologram, and thus the width of the reconstructed images is determined by the Heisenberg uncertainty relation. This is clearly the best that can be achieved in any holographic reconstruction, and the Gabor zone plate takes on the significance of being the hologram capable of reconstructing the smallest diffraction-limited spot image of a point object.

For the purpose of performing electron holography with atomic scatterers, of course, it is necessary to replace the isotropic scattering factor, f, in the above formulae with the atomic scattering factor, whose magnitude $|f|$ and phase δ are both functions of the scattering angle θ. For illustration, we plot in Fig. 2 the magnitude and phase of the "plane-wave" scattering factor

$$f(\theta)=\sum_{l,m} t_l Y^*_{lm}(\theta)Y_{lm}(\theta)\ . \tag{13}$$

of Cu for an electron energy of 914 eV. The corresponding diffraction pattern from a point emitter of electrons and a Cu atom placed at the same distance (2.55 Å) from

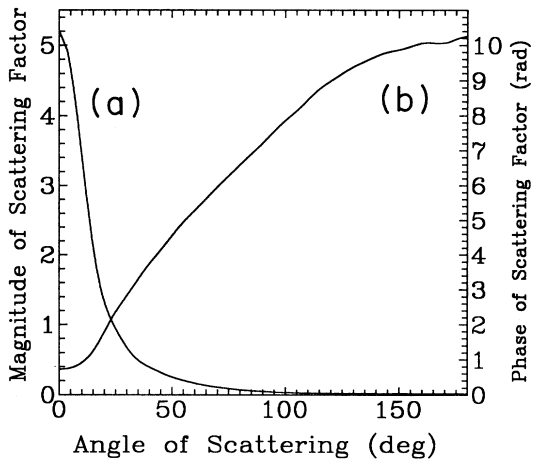

FIG. 2. Plot of the "plane wave" atomic scattering factor $f(\theta)$, for 914-eV electrons and a Cu scatterer at 300 K. The magnitude (a) shows the forward-scattering peak at 0° and very weak scattering near 180°. The rapid variation of the phase, $\arg[f(\theta)]$, plotted in (b), causes a shift of the atom position in the reconstruction.

the source as in our previous simulation [Fig. 1(a)] is shown in Fig. 1(b). Perhaps the most obvious difference with Fig. 1(a) is the appearance of a relatively much stronger central peak on the diffraction pattern. This is associated with the strongly forward-peaked nature of the electron scattering factors for atoms at such energies. Also note the existence of one extra fringe over the polar angle range 0–70°. This is a consequence of the angular variation of the phase of the scattering factor. The overall appearance of this diffraction pattern remains somewhat similar to that of the Gabor zone plate, however, and we term it an "atomic zone plate."

The so-called spherical-wave temperature-corrected scattering factor is not very different from the plane wave form (13), and in the former case the following parametrized forms were fitted[9] by a least-squares procedure:

$$|f(\theta)|=f_0 e^{-\alpha(1-\cos\theta)} \tag{14}$$

and

$$\delta(\theta)=\beta(1-\cos\theta)+\gamma\ , \tag{15}$$

where the values of $\alpha\sim 25$, $\gamma=1.8$, $\beta=5$, and $f_0=5$ a.u. were found. With this parametrized form, the reconstructed image intensity along the principal axis can likewise be calculated analytically from (9).[9] The resulting intensity takes the form

$$I(z)\propto F(z)+\frac{f_0}{z_0}\frac{\{1+e^{-2\alpha(1-c_m)}-2e^{-\alpha(1-c_m)}\cos[k(1-c_m)(z-z_i)]\}}{\alpha^2+k^2(z-z_i)^2} +\frac{f_0}{z_0}\frac{\{1+e^{-2\alpha(1-c_m)}-2e^{-\alpha(1-c_m)}\cos[k(1-c_m)(z+z_i)]\}}{\alpha^2+k^2(z+z_i)^2} \tag{16}$$

where

$$z_i=z_0+\beta/k \tag{17}$$

and $F(z)$ is a function centered on $z=0$. Equations (10) and (16) are the same as those given in our other paper[9] except that they have been generalized for arbitrary maximum polar angle of holographic data $\theta_{\max}$. In view of the high value of α the terms involving exponentials containing this quantity in (16) are negligible. Also as before, the quantity $F(z)$ is largely removed if χ replaces H in (9), and (16) reduces to the sum of the two Lorentians:

$$I(z)\propto\frac{1}{\alpha^2+k^2(z-z_i)^2}+\frac{1}{\alpha^2+k^2(z+z_i)^2}\ . \tag{18}$$

This intensity function peaks at $z=\pm z_i$, which is displaced further away from the emitter position than the true atom center z_0 by $\beta/k\simeq 0.3$ Å. Considering the simplifications of our analytical model, this is in reasonable agreement with the displacement observed on the function [Fig. 3(b)] calculated numerically from the diffraction data of Fig. 1(b). Also apparent from our analytical model is that the width of the peaks is approximately $2\alpha/k=3.2$ Å. This is in excellent agreement with the peak width observed on Fig. 3(b). Note that for the parameters chosen, the widths of these reconstructed atomic peaks are determined not by the maximum data collection angle $\theta_{\max}$, but by the parameter α which determines the angular width of the forward-scattering peak. The reason, of course, is that the angular range of useful data in this case is determined by the latter quantity rather than the former, since the amplitude of the holographic fringes dies out over a much smaller angular range than $\theta_{\max}$.

A physical way to understand the displacement of the image peak from the atomic zone plate away from the true atom position is by noting that the larger number of interference fringes in Fig. 1(b) compared with Fig. 1(a) approximates a Gabor zone plate due to a scatterer further away from the source. On the "forward-focusing" picture,[25] a scattering atom at such an energy is regarded as an imperfect lens for an incident electron beam, bringing it to a somewhat diffuse "focus" on the far side of the atom. The diffuse peak in the reconstructed intensity on the far side of the atom seen on Fig. 3(b) appears to lend

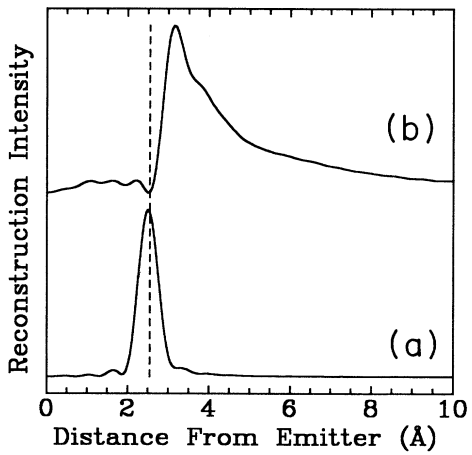

FIG. 3. Reconstructed images from the diffraction patterns of Figs. 1(a) and 1(b) along the line between source and emitter. (a) The Gabor zone plate reconstructs a narrow symmetric peak at the correct position of 2.55 Å (indicated by the vertical dashed line). (b) The reconstructed image from the atomic zone plate manifests a broader peak, moved to a position further from the emitter.

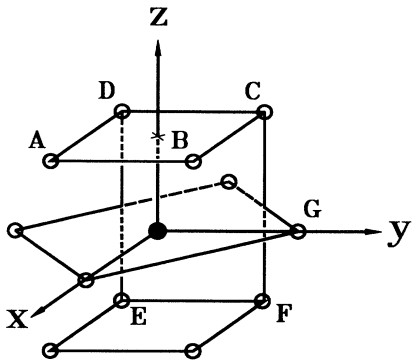

FIG. 4. Line diagram showing the positions of the 12 nearest-neighbors of an atom in the interior of a copper crystal. The crystal is oriented with the (100) plane perpendicular to the z axis. These atoms are labeled as referred to in the text.

support to such a view, since a holographic reconstruction process may be regarded as one which generates, in part, the time reverse of the wave scattered by that atom.

In the following calculations we will study the diffraction patterns of different subsets of the nearest neighbors of a copper atom in a face-centered-cubic copper crystal. To help visualize the geometry, we present in Fig. 4 a line diagram of all the nearest neighbors of an atom in the interior of the crystal. This crystal is oriented with the (100) plane perpendicular to the z axis. The following calculations will be for atoms in this orientation, where the detector is a portion of a sphere, in the half space of positive z, centered on the emitter, very distant from it. We shall refer to the atoms A,B,C,D, in the half space of positive z, as being "above" the emitter atom, the atoms $E,F,\ldots$ (negative z) as "below" the emitter atom, and the atoms $G,\ldots$ (in the plane $z=0$) as "in the plane of" the emitter atom.

IV. THE FORWARD-SCATTERING GEOMETRY

The diffraction pattern resulting from scattering from the four Cu atoms, A, B, C, and D, above the emitter is considered next. In Fig. 5(a) we show the pattern arising from isotropic scatterers, by setting to zero all the atomic phase shifts except the one corresponding to an angular momentum, $l=0$. Note the prevalence of overlapping interference fringes over the whole pattern. As we saw in the case of the Gabor zone plate, above, this is the ideal circumstance for good reconstructions of atomic positions, as shown in sections through the atoms parallel to their plane [Fig. 5(b)] and perpendicular to this plane, passing through atoms C, D, E, and F [Fig. 5(c)]. In Fig. 5(b), the crosses mark the positions of the atoms A and D and the reconstructed atomic positions are seen to be near perfect. In Fig. 5(c), crosses are placed at the positions of atoms D and E. The calculation had no atoms at the positions E and F, and yet the reconstructed image contains bright features at these positions. These are the "twin images" of the atoms B and A.[2,3] The three-dimensional images of the atoms are ellipsoidal rather than spherical. This effect is a consequence of the uncertainty principle:[6] the resolution parallel to a particular direction in the image is proportional to the inverse of the range of electron momenta associated with that direction in the hologram (i.e., $\Delta\alpha=2\pi/(k_\alpha^{\max}-k_\alpha^{\min})$,

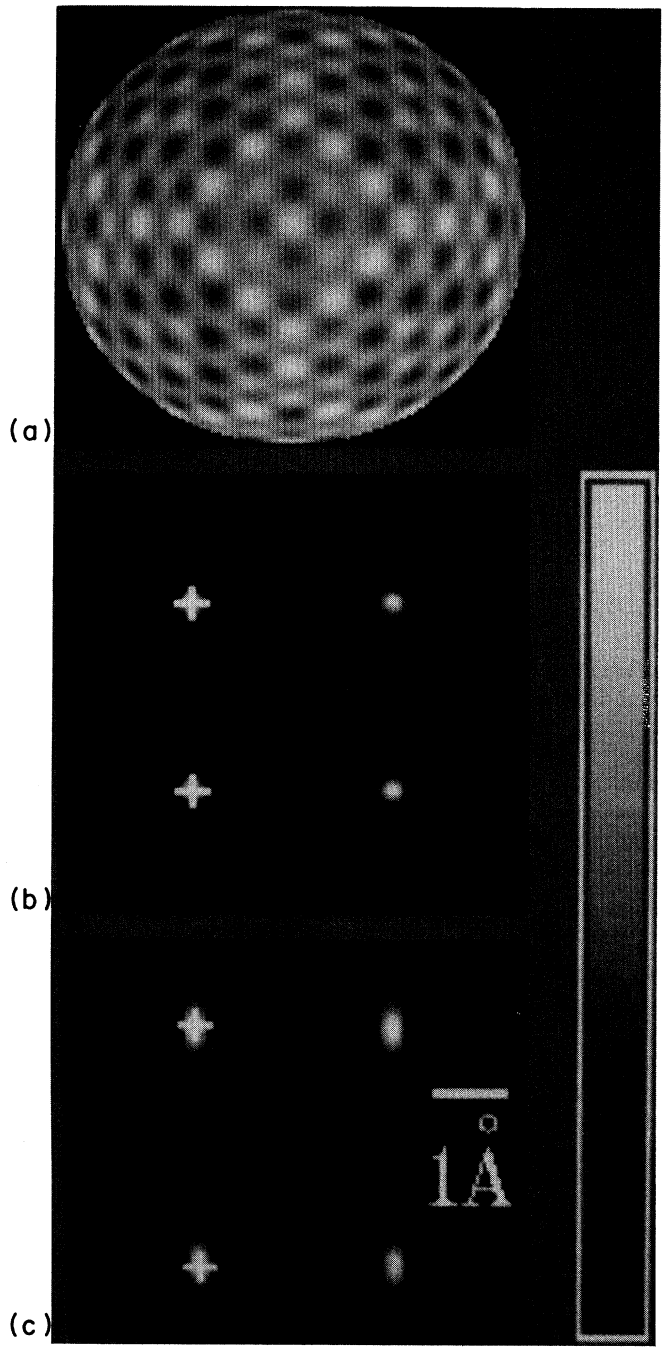

FIG. 5. (a) The diffraction pattern of four isotropic scatterers placed above the emitter. (b) and (c) contain sections of the reconstructed image from (a). Section (b) contains the four atoms A, B, C, and D of Fig. 4, and crosses mark the positions of atoms A and D. Section (c) contains the atoms C and D, and in the lower part of this section are the twin images of atoms B and A, which are found at the positions of atoms E and F. Crosses are placed at the positions of atoms D and E.

$\alpha=x,y,z$). Since our hologram is measured over a spherical cap, the resolution parallel to the axis of the cap is $\Delta z=2\pi/[k(1-\cos\theta)]$, while perpendicular to this direction, the resolution is $\Delta x,\Delta y=2\pi/(2k\sin\theta)$. Thus, the resolution parallel to the axis of the cap is always poorer than that perpendicular to this axis (in the cases here, by about a factor of 3), giving the atoms an ellipsoidal shape.

The corresponding diffraction pattern for more realistic atom scatterers, with their full scattering factors, is shown in Fig. 6(a). This is a model of a diffraction pattern due to Auger electrons emitted from atoms in the subsurface layer of a two-monolayer thin film, since forward scattering dominates the pattern. Note the prominent forward-scattering peaks. The patterns also suggest that the holographic fringes radiating from each forward-focusing peak may lose visibility within a small angle from those peaks. From the holographic point of view, this implies that the relevant zone plate may have a much smaller angular range, centered around the forward-scattering direction. The corresponding sections through the reconstructed images are shown in Figs. 6(b) and 6(c).

In these reconstructed images we note several new effects. First, the ellipsoidal shape of the atomic images of Fig. 6(c) is exaggerated and the axis of the ellipsoid is now oriented along the forward scattering direction. Second, there are high-intensity artifacts shown near the centers of Figs. 6(b) and 6(c). These effects have been seen in reconstructed images from experimental diffraction patters.[5,6] Since it is well known that, at high kinetic energies, only small-angle atomic scattering is important, this diffraction pattern is dominated by single scattering, and therefore the origin of these effects is most unlikely to be multiple scattering as such. Rather, the cause is likely to be found in the peculiar form of the high-energy atomic-scattering factors.

The tubular shape of the reconstructed atomic images[5,6] is caused by the angular dependence of both the magnitude and phase of the scattering factor of the atom under study, as mentioned in our discussion of Fig. 3(b). Because the fringe intensity is significant only over a narrow angular range, centered about the forward-scattering direction, the relevant zone plates for the atoms are effectively truncated at some maximum angle from this direction. Applying the same resolution arguments as above, we see that the atom image width will be a maximum parallel to the forward-scattering direction.

For comparison with the single-atom case in Fig. 3, we plot in Fig. 7(a) the intensity along a straight line through the position of the electron source and that of a scattering atom (say A of Fig. 4) on the reconstructed image. We have termed the function represented by such a graph a "radial image function," or RIF for short. This RIF looks similar to that of Fig. 3(b) except for the high-intensity features at small radius, a particularly bright feature occurring at 0.8 Å. The origin of such a feature has been observed to be associated with the forward-scattering peaks on the diffraction patterns.[32] We now offer a physical explanation of this observation.

We have already seen that a Gabor zone plate is capable of generating a sharp peak on a RIF. If the image artifact at $r=0.8$ Å were due to some kind of artificial Gabor zone plate on the diffraction pattern, then according to (7) that zone plate must possess a bright fringe at an angle of $\theta=60°$ away from the radial direction being considered (assuming $k=15.5$ Å^{-1} corresponding to an energy of 914 eV), remembering that the $\theta=0$ bright spot

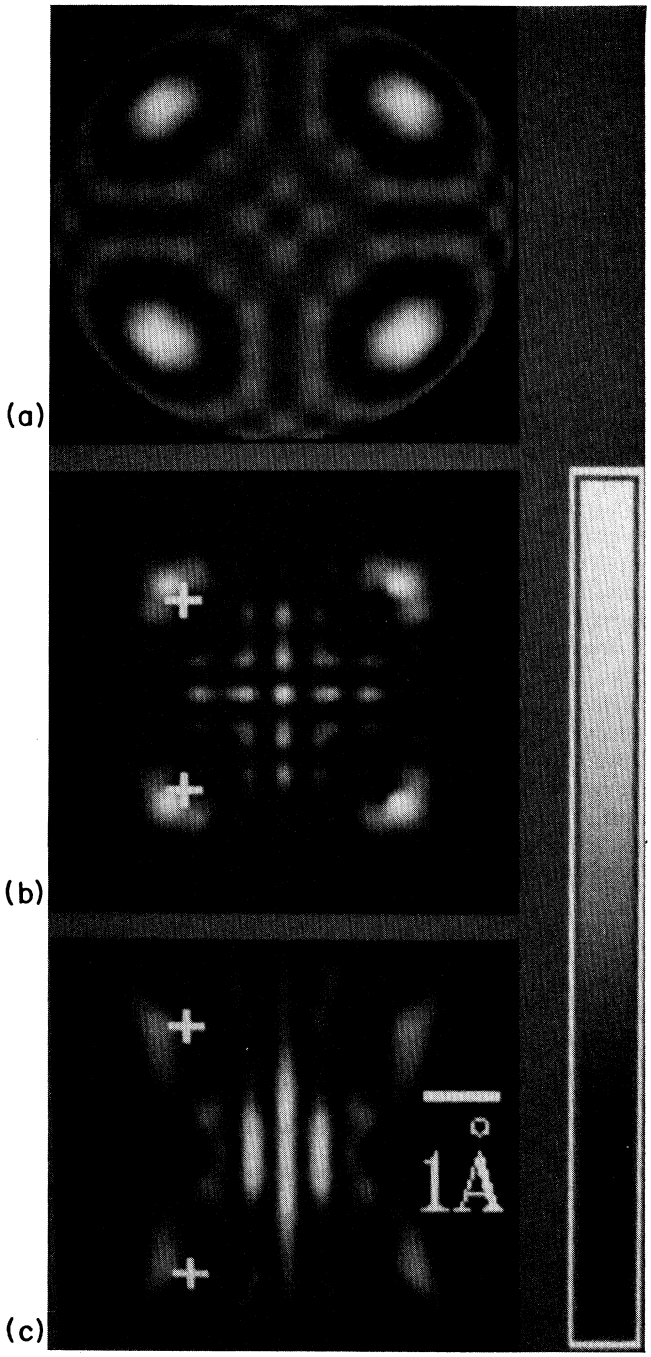

FIG. 6. The diffraction pattern and reconstructed images for copper atoms in the same geometry as for Fig. 5. The reconstructed images of the atoms appear distorted and shifted to larger distances from the emitter atom. Also seen are artifacts, away from atom positions, due to the forward-scattering features in the diffraction pattern.

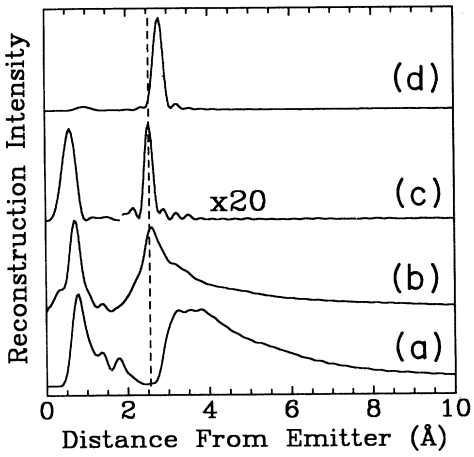

FIG. 7. Reconstructed intensity along the line joining the emitter and atom A: (a) for Fig. 6(a); (b) same as (a) but using a new reconstruction technique, which deconvolves the phase the scattering factor; (c) same as (b), but now deconvolving both the magnitude and phase of the scattering factor. Curve (d) is the reconstructed intensity along the line passing through atom E of Fig. 4, for the back-scattering diffraction pattern of Fig. 12(b).

is assured in this case by the forward-scattering effect of a real atom along the direction of our radial image function (corresponding to a phase $\delta=0$). But 60° is precisely the angle between the forward-scattering peak of the atom A and that of a neighboring scattering atom, such as B. Thus, the forward-scattering peaks due to other atoms may be considered to generate a crude pseudo-Gabor zone plate centered on the forward-scattering direction of atom a, to give rise to the artifact seen on the reconstructed image.

At first sight, the above analogy with the Gabor zone plate may sound somewhat farfetched in view of the strong azimuthal variation, about the direction of the RIF in question, of the intensity associated with the other forward-scattering peaks on the diffraction pattern. That this is not the case may be seen by realizing that the amplitude RIF in an arbitrary direction may be written as a generalization of (9) if the polar axis is now taken along that RIF:

$$A(z)=-\int J(\theta)\exp(-ikr\cos\theta)d(\cos\theta)\ , \tag{19}$$

where

$$J(\theta)=\int H(\theta,\phi)d\phi\ . \tag{20}$$

Thus the amplitude RIF, $A(z)$, can be written as a *one-dimensional Fourier transform* of the azimuthally-integrated polar angle variation of the holographic intensity. Hence the azimuthal variation about the RIF direction is of *no consequence* for the form of the RIF, a fact that emphasizes the utility to the zone-plate model above.

The realization that forward-scattering features on diffraction patterns do not in themselves carry holographic information but that, on the contrary, they act to degrade the crystallographic fidelity of the reconstructed images suggests the possibility of a more sophisticated reconstruction algorithm than (8), at least in the case where the form of a diffraction pattern is due mainly to single-scattering processes. We examine this possibility in Sec. IV A.

A. A deconvolution algorithm for locating the atom centers

We have already noted that a Gabor zone plate reconstructs the image of an atom much more faithfully than the corresponding atomic zone plate. We see this apparent shift even in the presence of many scattering atoms (see Fig. 6). The question then arises whether, in electron emission holography, it would be possible to recover the optimal holographic properties of superposed Gabor zone plates for the accurate reconstruction of true atomic positions. A clue to such a scheme is found by considering the kinematic expression for the intensity of the diffraction pattern due to an s-wave emitter and several scattering atoms, specified by the index i:

$$I(\mathbf{k})=\text{const}\times\left|1+\sum_i f(\gamma_i)\exp[i(kr_i-\mathbf{k}\cdot\mathbf{r}_i)]/r_i\right|^2\ , \tag{21}$$

where

$$\gamma_i=\hat{\mathbf{k}}\cdot\hat{\mathbf{r}}_i\ . \tag{22}$$

An equation of this form also holds when multiple scattering is present if $f(\gamma)$ is generalized to take into account all scattering paths that end on the atom i.[18] Expanding the square, Eq. (21) may be written

$$I(\mathbf{k})=\text{const}\times\left[1+\sum_i|f(\gamma_i)|^2r_i^{-2}+\left[\sum_i f^*(\gamma_i)\exp[i(\mathbf{k}\cdot\mathbf{r}_i-kr_i)]/r_i+\text{c.c.}\right]\cdots\right.$$
$$\left.+\sum_{i\neq j}f^*(\gamma_i)f(\gamma_j)\exp[-ik(r_i-r_j)+i\mathbf{k}\cdot(\mathbf{r}_i-\mathbf{r}_j)]/(r_ir_j)\right]\ . \tag{23}$$

According to Barton's[2] argument, the term linear in $f^*(\gamma_i)$ gives rise to peaks in the reconstructed intensity $|A(\mathbf{r})|^2$ when $\mathbf{r}=\mathbf{r}_i$, the true positions of the atom centers, if the Helmholtz-Kirchoff algorithm (8) is employed, by virtue of a stationary-phase condition. The same argument suggests that the complex conjugate of the above term in $I(\mathbf{k})$ gives rise to a peak at the position of the "twin" image $\mathbf{r}=-\mathbf{r}_i$. This argument is based on

the assumption that $f(\gamma_i)$ and its complex conjugate vary much more slowly with $\hat{\mathbf{k}}$ than the exponential terms multiplying them in (23). Both arguments are exact in the case of an isotropic scatterer [for which $f(\gamma_i)$ is a constant], which gives rise to superimposed Gabor zone plates. When the angular dependence of f cannot be neglected, the reconstructed image contains a component that may be regarded as the convolution of the true positions of the atomic cores with the Fourier transform of the relevant atomic scattering factors. This suggests the following deconvolution algorithm[11] for extracting the crystallographic information, namely the true positions of the atoms.

$$A(\mathbf{r}) = \int [I(\mathbf{k})/f^*(\hat{\mathbf{k}}\cdot\hat{\mathbf{r}})]\exp(-ik\hat{\mathbf{k}}\cdot\mathbf{r})d\hat{\mathbf{k}} \ . \quad (24)$$

Substituting (23) into (24), we see that the expression for $A(\mathbf{r})$ contains the term

$$\sum_i (1/r_i)\exp(-ikr_i)\int [f^*(\hat{\mathbf{k}}\cdot\hat{\mathbf{r}}_i)/f^*(\hat{\mathbf{k}}\cdot\hat{\mathbf{r}})] \times \exp[ik\hat{\mathbf{k}}\cdot(\mathbf{r}_i-\mathbf{r})]d\hat{\mathbf{k}} \ , \quad (25)$$

which recovers an exact stationary-phase condition for the atom positions, precisely as in the case of the Gabor zone plate. Note also that the division of $I(\hat{\mathbf{k}})$ by the highly forward-peaked function f^* also has the beneficial effect of reducing the forward bias of the holographic fringe distribution, increasing the effective angular range of the holographic data and thereby improving image resolution.

Another desirable byproduct of our deconvolution of f^* is that although the stationary-phase condition is enhanced for the true atom image, it is diminished for the twin. The only remaining practical question is the form chosen for f. In the case where just a single layer of atoms lie between source and emitter, we believe it is reasonably well approximated by the expression for the kinematic "plane-wave" atomic scattering factor (13). Using this form, we have implemented our deconvolution algorithm (24) for image reconstruction. The results are illustrated in Figures 7, 8, and 9. If we replace $f^*(\hat{\mathbf{f}}\cdot\hat{\mathbf{r}})$ in (24), by $\exp\{i\arg[f^*(\hat{\mathbf{k}}\cdot\hat{\mathbf{r}})]\}$, we "remove" only the phases of the relevant (complex conjugate) atomic scattering factors in (23). Figure 8 shows the resulting image. The corresponding line plot is shown in Fig. 7(b). In comparison with the reconstructed images in Fig. 6, we see that the image peaks are moved back to the true atom positions, and that the peak asymmetry and interatomic artifacts are significantly reduced, especially in the planar sections. However, there remains some asymmetry of the atom images about the exact positions of the atoms. Also, the twin images, visible in the lower part of Fig. 8(b) are no longer symmetric with respect to the true images. This is due to the fact that, at the positions of the twins, the diffraction pattern is divided by the complex exponential of the phase of the *back*-scattering, rather than the forward-scattering factor.

In Fig. 9, we show the plane of constant z through the atoms A, B, C, and D in the image resulting from a full implementation of our new algorithm (24). This results in the "removal" of both the amplitude and phase of the relevant atomic scattering factors in the single-scattering

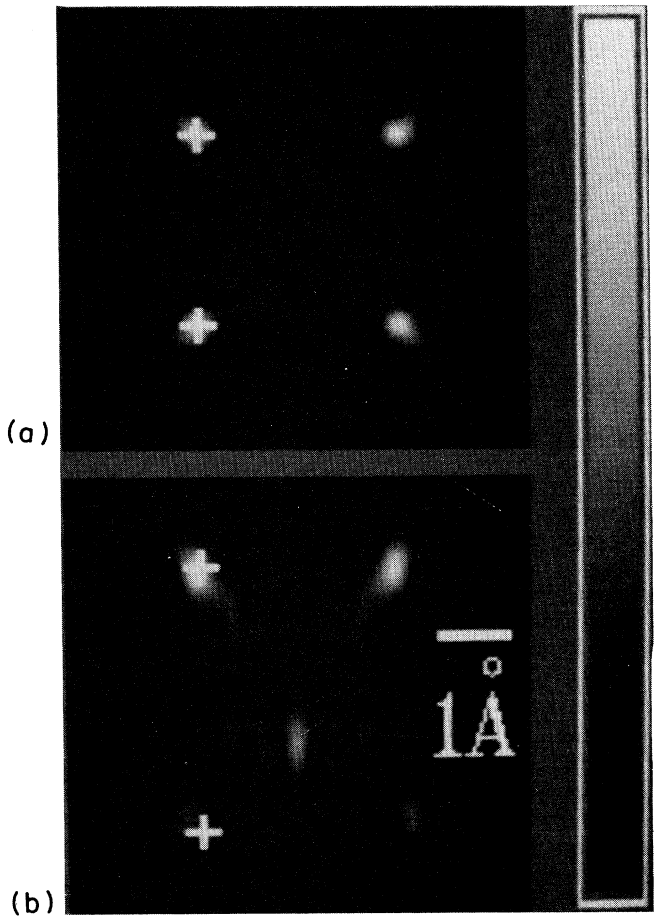

FIG. 8. The reconstructed intensity from the diffraction pattern of Fig. 6(a) in (a) the *ABCD* plane, and (b) the *CDEF* plane of Fig. 4 using the reconstruction scheme, which compensates for the phase of the atomic scattering factor. The images are shifted back to their true positions but still appear asymmetric.

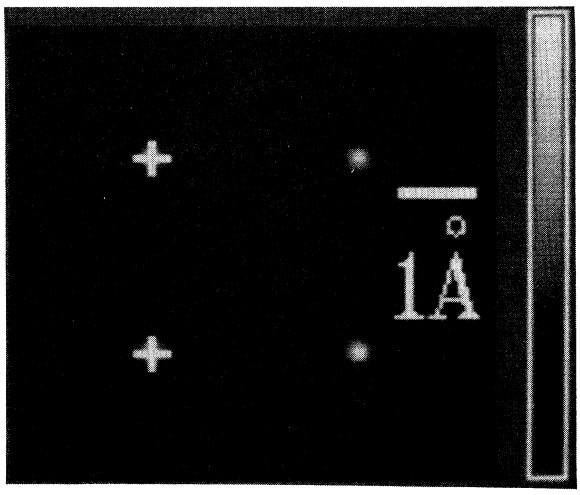

FIG. 9. Same as Fig. 8(a), but here using the reconstruction algorithm, which deconvolves the full atomic scattering factor from the image.

terms in (23). In this plane the atoms appear symmetric and are so sharply peaked that they completely dominate the artifacts near the z axis. The corresponding line plot is shown in Fig. 7(c). Here too we see that the atom image is symmetric, but because the forward-scattering magnitude is large, division by this factor reduces the peak height relative to images due to backscattering and to the small radius artifacts. We have not shown the section of constant x for this case because the part of the image with negative z has been divided by the small backscattering amplitude and therefore dominates this section.

At this point we would like to comment on the relative merits of our modified reconstruction scheme and one proposed recently by Tong *et al.*[10] Both schemes address the same problem, namely, an optimum extraction of structural information from a diffraction pattern by eliminating effects arising from the details of the atomic potentials, as manifested by the angular variations of the phases and amplitudes of the atomic scattering factors. However, there are significant differences. The method of Tong *et al.*[10] involves the division of the intensity enhancement function $\chi(\hat{\mathbf{k}})=[I(\hat{\mathbf{k}})-A]/A$ [where A is the angle-averaged value of $I(\hat{\mathbf{k}})$] by a function of $\hat{\mathbf{k}}$ *only*, which individually corrects χ by the amplitude and phase of the atomic scattering factor along a particular forward-scattering direction. One problem with this is that the forward-scattering directions have to be identified from the diffraction pattern. This is often difficult due to the presence of the so-called "diffraction peaks," which may be as intense as the forward-scattering peaks (see, e.g., the Auger diffraction pattern in Fig. 11). Even if the forward-scattering directions were identified, the resulting reconstructed "images" are each meaningful only along those particular directions. The authors[10] propose the creation of a composite image from radial image functions along the different forward-scattering directions, although none is shown in their article. Instead, we propose dividing the diffraction pattern by a test function representing the angular variation of the scattering factor of an atom placed at the position of image point *currently being calculated.* That is, we divide by a function of both reciprocal space ($\hat{\mathbf{k}}$) and real space ($\mathbf{r}$). By this means we obtain a meaningful three-dimensional image *in one step,* without a prior knowledge of the forward-scattering directions.

B. Multiple scattering, intermodulation noise, and autocorrelation

When electrons are emitted from atoms in a layer immediately below the outermost surface layer, the strongly forward-peaked nature of the atomic scattering factors results in a measured diffraction pattern being dominated by interference between the direct (or reference) wave and *single*-scattering paths. If the electron sources were deeper within the crystal, the number of significant multiple-scattering paths increases. It is important to analyze the effects of such multiple scattering and other many-atom effects. We note that, the first successful experiments on holography with local reference waves[5,6] involved incoherent electrons emitted from many layers of atoms near a single-crystal surface, a circumstance in which multiple scattering must be expected to play a significant role. Unlike the configurations discussed above, in the single-crystal case the Helmholtz-Kirchoff algorithm (8) was found to reproduce the true atom positions on the reconstructed image, without the need for the deconvolution procedure discussed in Sec. IV A. We suggest the following explanations of this effect.

We may regard the kinematic expression (23) for the diffracted intensity as the first four terms of a multiple-scattering series expansion; the next two terms, due to double scattering, being approximately:

$$\sum_{i\neq 0}\sum_{j\neq i} f^*(\hat{\mathbf{k}}\cdot(\mathbf{r}_j \hat{-} \mathbf{r}_i))f^*(\hat{\mathbf{r}}_j\cdot\hat{\mathbf{r}}_i)\exp[-i\mathbf{k}\cdot\mathbf{r}_j - ik(|\mathbf{r}_j-\mathbf{r}_i|-r_i)]/(|\mathbf{r}_j-\mathbf{r}_i|r_i)+\text{c.c.} \tag{26}$$

These and higher-order scattering terms have different and more complicated prefactors to the exponential, $e^{i\mathbf{k}\cdot\mathbf{r}_j}$, than the direct term [the third term of Eq. (23)]. Thus, if enough of these terms have sufficient magnitude, the phases of these prefactors tend to be randomized, and their amplitudes tend to become more isotropic, conditions that favor the faithful reconstruction of the true atom positions by means of the Helmholtz-Kirchhoff algorithm (8).

When the reference wave is scattered by a large number of atoms in a crystal the fourth term in Eq. (23) may also play a role in the image formation. In conventional holography, this term gives rise to what is known as "intermodulation noise",[29] which acts essentially to degrade the image. However, in the special case where the objects (in our case the scattering atoms) form a Bravais lattice, this circumstance may act to reinforce the image. We can appreciate this by noticing that application of the Helmholtz-Kirchoff algorithm (8) to this term results in approximate stationary-phase conditions when $\mathbf{r}=\mathbf{r}_i-\mathbf{r}_j$. The resulting image would be an autocorrelation of the atomic structure. Such a process is quite analogous to the generation of a Patterson function in x-ray crystallography.[33] In the case of a Bravais lattice, the peaks of the Patterson function are coincident with the true atom positions, and the intermodulation noise actually acts to reinforce the image of the lattice. In the case of atomic clusters with no long-range order, extra peaks may appear on the reconstructed image, corresponding to distances $\mathbf{r}_i-\mathbf{r}_j$ from the source if the higher-order terms are strong enough. Thevuthasan *et al.*[34] have termed these peaks "self-images." It has also been pointed out,[35] that in emission electron holography, independent of the details of the scattering, a Fourier-transform algorithm reconstructs an autocorrelation of the wave function of the emitted electron.

To summarize, from the point of view of the use of x-ray photoelectron holography for studies of epitaxial growth, it would appear that, in the case of ultrathin films, or that of an emitter atom in a molecule adsorbed on a surface, a deconvolution algorithm, like that discussed in Sec. IV A, is necessary, but for single-crystal surfaces the Helmholtz-Kirchoff algorithm[2] is more appropriate, although in that case the atomic images are broadened and elongated in the forward-scattering directions.

In intermediate cases, it may be helpful to combine our algorithm, (24), which improves fidelity of the parts of the reconstructed atomic images due to single scattering, with one, suggested recently by Barton,[36] for enhancing the contributions to the image of the single-scattering terms by combining the data from diffraction patterns from electrons of several energies. The combined algorithm could be written

$$A(\mathbf{r})=\int\int [I(k,\hat{\mathbf{k}})/f^{*}(k,\hat{\mathbf{k}}\cdot\hat{\mathbf{r}})]e^{ikr}e^{-ik\hat{\mathbf{k}}\cdot\mathbf{r}}d\hat{\mathbf{k}}\,dk \ . \quad (27)$$

C. The localization of the holographic fringes

A further important aspect of holography in our forward-scattering geometry is illustrated in Fig. 10(a). Here we have artificially removed the intensity from the upper left-hand quadrant of Fig. 6(a), and the resulting sections through the reconstructed image are shown in Figs. 10(b) and 10(c). Note the disappearance of the image of the atom D, giving rise to the forward-scattering feature within the blocked-out section. This is an unexpected result to those familiar with optical holograms, where the removal of part of a hologram causes some loss of resolution, but does not lead to the preferential removal from the image of some particular localized object. Our observation is a clear indication that in the forward-scattering geometry, strong holographic fringes associated with a particular atom are found only in the near vicinity of the forward-scattering peak associated with that particular atom.

The validity of this result is further reinforced by the observation of the same effect on a measured diffraction pattern [Fig. 11(a)] from an experiment with 914-eV Auger electrons from a Cu(100) surface. Figures 11(b) and 11(c) are the sections through the reconstructed image corresponding to Figs. 10(a) and 11(b), respectively, on the calculated holograms. The relative displacements of the nearest-neighbor scatterers from the sources in the experimental sample are the same as in the model calculations above. We point out here that this experimental data is new and is an improved dataset with higher signal-to-noise ratio than was previously published.[6]

These results must not be taken to imply that useful holographic information about any particular atom is not found over the whole of the hologram. In fact, if the forward-scattering peaks were removed by a Fourier filtering technique,[37] the weaker holographic fringes further away from the forward-scattering direction may be recovered and usefully employed for reconstruction purposes.

Conversely, it should be noted that a reconstruction algorithm for a single hologram which restricts its scope of operation to data on a limited angular range around the forward-scattering direction must suffer from a severely reduced resolution on the reconstructed image, according to Abbe's theory.[31]

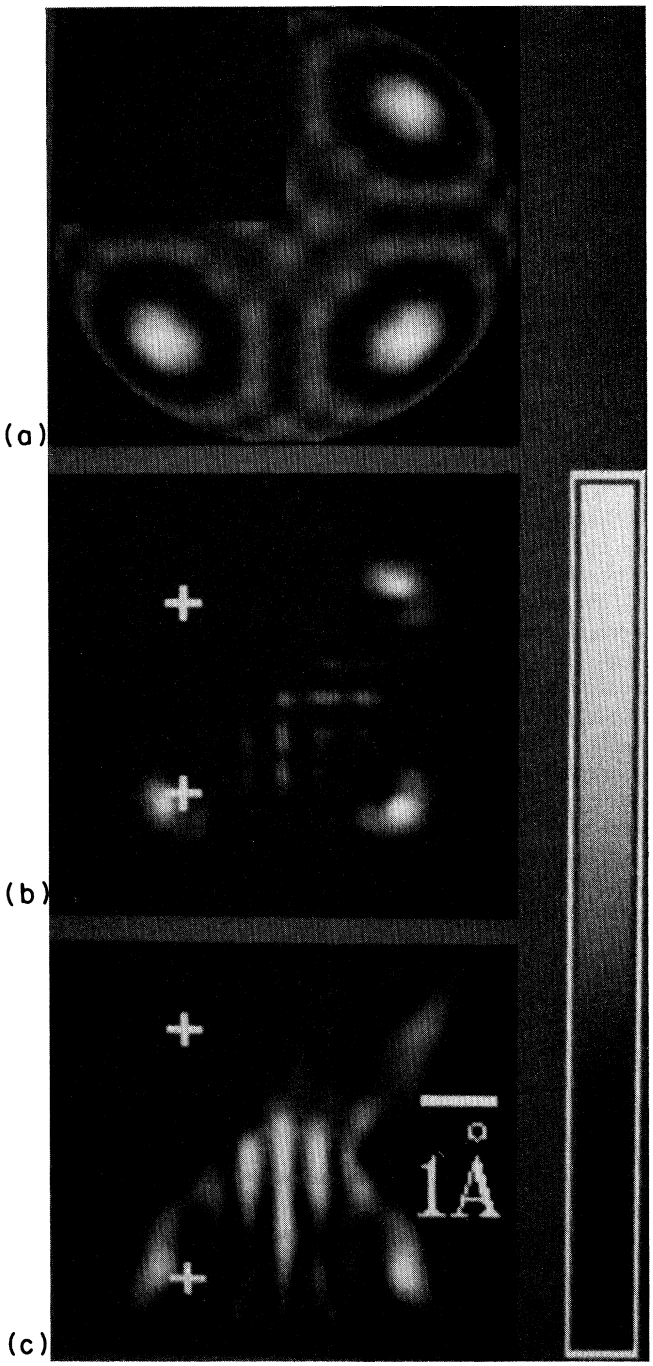

FIG. 10. (a) The diffraction pattern of Fig. 6, where we have blocked out one quarter of the data and (b) and (c) the same planar sections through the reconstructed image as in Fig. 6. We see the unexpected result that the atom D appears to be missing from the reconstruction. Forward scattering causes most of the measurable holographic fringes of an atom to be localized in a small part of the diffraction pattern. Thus, unlike optical holography, excising a part of a forward scattering hologram may remove specific features from its reconstruction.

V. THE BACKSCATTERING GEOMETRY: EFFECTS OF THERMAL VIBRATIONS

An advantage of the forward-scattering geometry for atomic-resolution holography is that the waves from the scattering atoms are not small, and hence give appreciable and easily measurable fringes on interference with the wave from the source. Its disadvantages are the appearance of the strong forward-scattering peaks, which give rise to interatomic artifacts, as well as the strong angular variation of the phase of the atomic scattering factor, which give rise to shifted atom images. This may necessitate the deconvolution of the effects of the nonisotropic atomic scattering factors from the reconstructed image. The first computer simulations of electron holography from local electron sources[2,3] concerned source atoms adsorbed on crystal surfaces, and it is important to compare our results above with those that might be expected in the "backscattering" geometry.

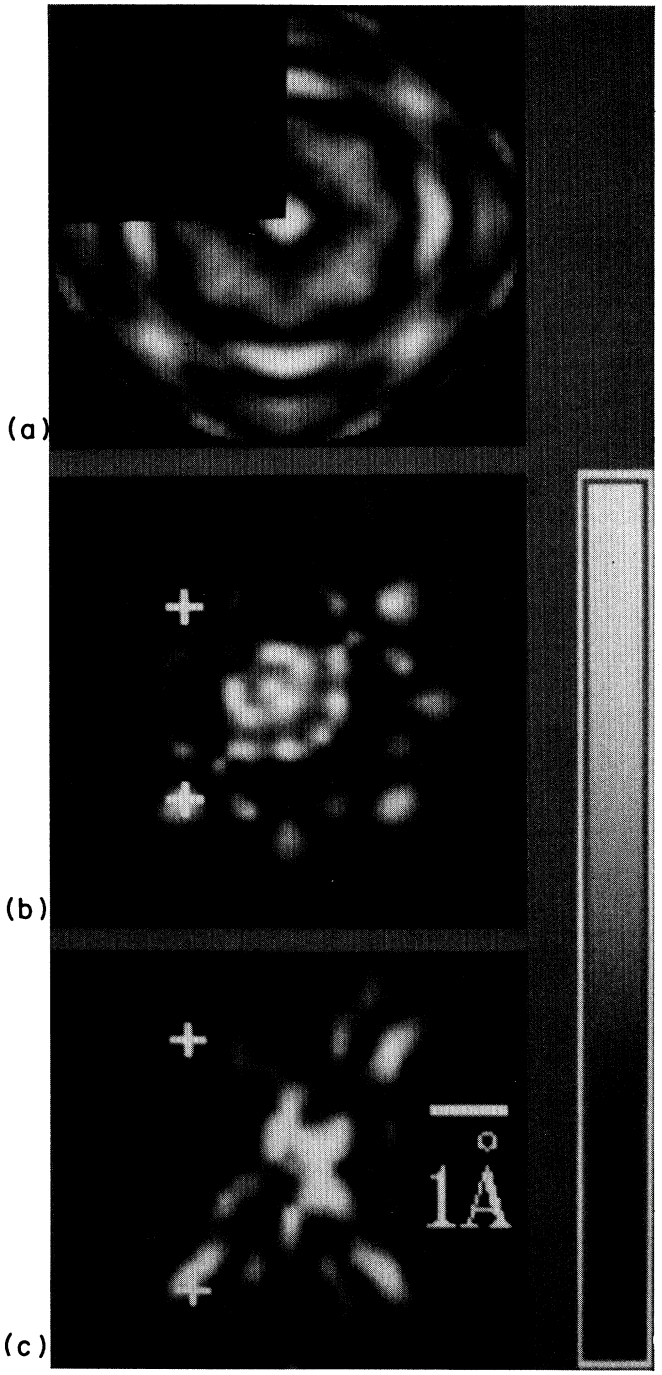

FIG. 11. We have performed the process of Fig. 10 on new Cu(100) single crystal Auger data to show this effect is reproduced using experimental data.

In the backscattering geometry, the scattering atoms are found at greater distances from the detector than the source. As a result, holographic fringes result from the interference between the electrons direct from the source, and those which suffer backscattering from the nearby atoms. The first and most obvious effect is that the visibility of the holographic fringes is much lower. Not only is the atomic back-scattering factor much smaller than the forward-scattering factor at such energies, the high momentum transfer in the scattering process also causes the Debye-Waller factors to be severely reduced.

However, if we examine, in Fig. 2, the nature of the back-scattering part of the atomic scattering factor, (i.e., for scattering angles between 90° and 180°), we notice that it varies much less rapidly in both amplitude and phase than its forward-scattering counterpart. That is, the parts of Figs. 2(a) and 2(b) near $\theta=180°$ are much more slowly varying than those near $\theta=0°$. Therefore diffraction patterns due to back scattering might be expected to yield good reconstructed images even with the Helmholtz-Kirchoff algorithm (8). A simulated pattern in this geometry is shown in Fig. 12(a), where only the four nearest-neighbor atoms below the emitter are used in the calculation (atoms $E,F,\ldots$ in Fig. 4). We see that the fringes are so weak as to be hardly noticeable. More quantitatively, if we define the contrast in a diffraction pattern as the difference between the maximum and minimum intensity divided by the average intensity in the pattern, the back-scattering diffraction pattern has only 7% of the contrast of that of Fig. 6(a). This kind of signal to background ratio is inaccessible to present measurement techniques.

The situation is much improved when the same pattern is calculated for a sample at 100 K. As indicated in Fig. 12(b), the contrast at 100 K is 25% of that in the forward-scattering geometry. The measurement of holographic fringes from an experiment in this case would be difficult but probably not impossible. The images reconstructed from this pattern, using the Helmholtz-Kirchoff algorithm (8), are shown in Figs. 13(a) and 13(b). Note the excellent reproduction of the atom positions on the image. In this case the hologram much more resembles that for the *s*-wave scatterers of Fig. 5, and the holographic fringes are distributed much more evenly over the whole of the diffraction pattern. The variation of the image intensity along a straight line from the source to the scattering atom is shown in Fig. 7(d). Here we see that the atom peak is sharp and symmetric, but shifted slightly (by 0.15 Å) from its true position. This shift is

caused by the relatively small angular variation of the phase of the atomic back-scattering factor. The electron back-scattering factor contains a small but non-negligible angular variation, and we find, even in this geometry, our deconvolution algorithm (24) noticeably improves the fidelity of the reconstructed image.

A further point of interest is the absence of small radius artifacts in both sections through the reconstructed image and in the line plot of Fig. 7(d). This is further support for our assertion that such artifacts are caused by the forward-scattering peaks on diffraction patterns.

On the basis of these data, we see that if the experimental difficulties of low holographic fringe contrast were overcome, the back-scattering geometry may well become an attractive one for electron holography of atomic structures. We note that the diffraction pattern shown here is a model for an adsorbate system at very low coverages.

In the case of a single-monolayer-thin film, such as copper on nickel, using Auger emission from copper atoms, the emitter would also be surrounded by copper atoms in the $z=0$ plane. These atoms are likely to give stronger fringes than those from the substrate, and may make possible the reconstruction of the nearby copper atoms in that plane. One may also improve the contrast in the diffraction pattern by using a substrate of high atomic number (such as tungsten) to increase the back-scattering cross section, or a substrate with a higher Debye temperature, to minimize Debye-Waller losses. Another way to improve the backscattering fringe contrast would be to use a lower electron kinetic energy to make the measurement.[2,3] However, this has the drawback of reducing the image resolution.[3]

VI. THE COEXISTENCE OF FORWARD AND BACK SCATTERING

Comparing the visibility of the holographic fringes in Figs. 6(a) and 12(a) it might be expected that, when forward and back scattering coexist, the fringes due to the latter may be overwhelmed by the former. As a final test of this we show, in Fig. 14, the calculated diffraction pattern from an emitter surrounded by all 12 nearest-

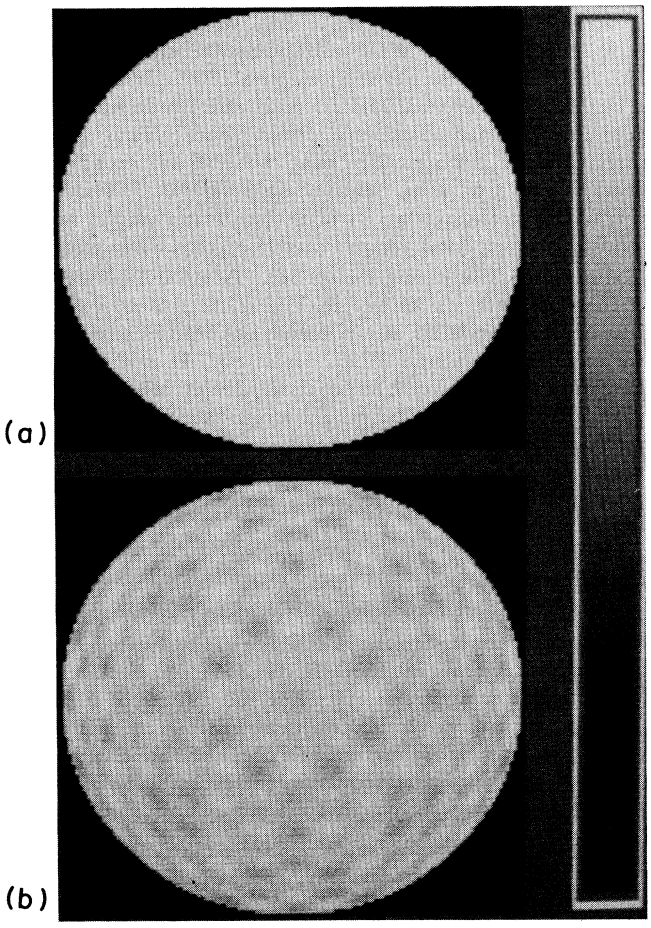

FIG. 12. Back-scattering diffraction patterns for a copper atom emitter with four copper atoms below it, at 300 K (a) and 100 K (b). The holographic fringes are practically immeasurable in (a) but may be measurable in (b), where the contrast is about 25% of that in Fig. 6(a).

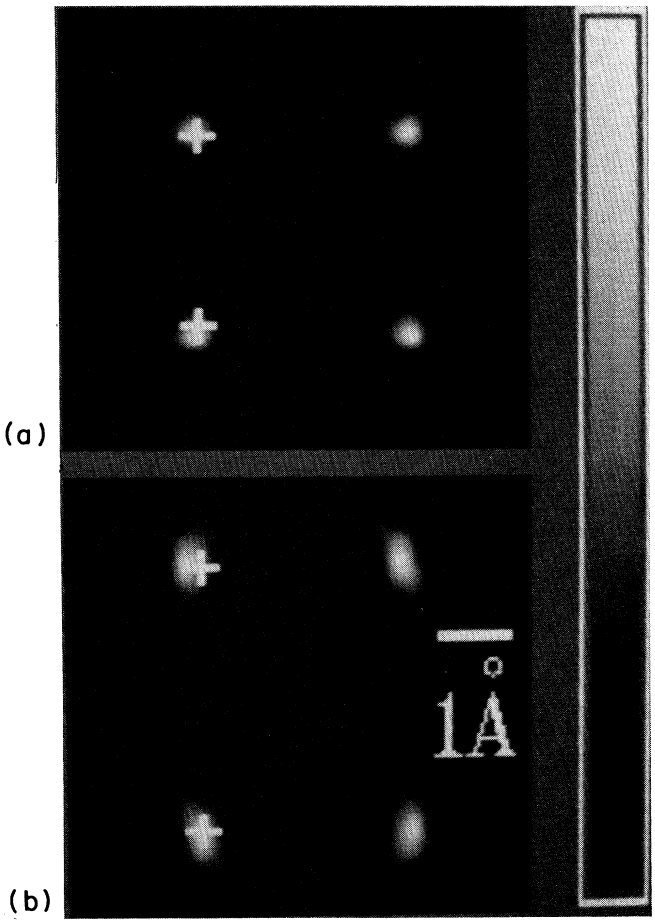

FIG. 13. The same sections through the reconstructed image from the diffraction pattern of Fig. 12(b) as in Fig. 5. Back-scattering patterns give sharp, artifact-free images, and this would be a desirable geometry for electron holography if the problems of the signal level could be overcome.

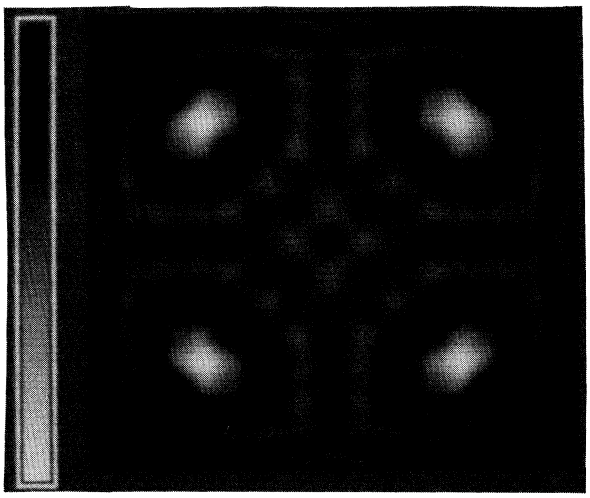

FIG. 14. The diffraction pattern from an emitter surrounded by all 12 of its nearest neighbors. This pattern is very similar to that of Fig. 6(a), showing that the four atoms that are situated between the emitter and the detector are the most important in determining the diffraction pattern.

neighbor atoms, that is, all the scattering atoms shown in Fig. 4. Comparing this with Fig. 6(a), we see that the difference between a cluster containing the four atoms above the emitter and one containing all 12 nearest-neighbor atoms is detectable but not very noticeable. Furthermore, image reconstructions from the latter pattern are practically indistinguishable from those of the former. In the plane of the emitter the forward-scattering artifacts dominate, and it is impossible to see the in-plane scattering atoms. This result agrees with experiments performed on single-crystal samples.

VII. CONCLUSIONS

Using a full multiple-scattering cluster calculation, including the effects of thermal vibration, we have investigated the holographic properties of electron diffraction patterns formed by atomic sources of electrons. These electrons are surrounded by nearby atoms, which scatter the emitted electrons so as to generate an interference pattern in the far field with the direct waves from the sources. Cluster models perhaps are the most convenient ones for isolating the elements of the complex multiple-scattering processes, which take place in a real experiment because of the facility they offer for selectively studying the contributions of individual atoms or groups thereof.

We find that the strongly peaked and angle-dependent forward-scattering factor localizes the measurable holographic fringes of an atom to a narrow angular cone centered about the forward-scattering direction. This scattering-factor can also shift the apparent atomic positions in the reconstructed images and elongate the atomic images along the forward-scattering direction. It is also indirectly the cause of high-intensity interatomic artifacts in the reconstructed images because forward-scattering features from neighboring atoms may behave as unphysical pseudoholographic fringes. A deconvolution algorithm, which corrects for the amplitude and phase variation of the atomic-scattering factor, is found to be more appropriate for forward-scattering holography when multiple-atom scattering effects are not too dominant. When scattering due to many atoms is important, the Helmholtz-Kirchoff reconstruction algorithm[2] is found to be adequate, as was shown in the case of experimental Kikuchi and Auger diffraction patterns from the surfaces of bulk crystals.[5,6]

For electrons of energies of the order of 1000 eV, back-scattering effects are found to be very weak compared with those due to forward scattering at room temperature, and back scattering contributes little to diffraction patterns containing forward-scattering features. However, at 100 K it may be possible to measure a back-scattering pattern from an adsorbed overlayer on copper, even at such energies. Reconstructing images from such back-scattering patterns with the use of the Fourier transform algorithm gives rise to bright peaks associated with the atoms, with few noncrystallographic artifacts. Nevertheless, even in this case, our deconvolution algorithm leads to more accurate bond length determinations.

In one of his earliest papers on the subject Gabor[38] described holography as a form of "diffraction microscopy," which he hoped would ultimately lead to the imaging of atomic structures. He proposed the use of an external source of electrons, a macroscopic distance from the objects studied, a geometry that places quite severe demands on electron coherence lengths. Using, as reference waves, electrons emanating from atoms within the sample[1] overcomes this difficulty. The resulting "images" are, of course, averages of the atomic structures surrounding all the emitters contributing to the measured diffraction pattern, and therefore are most useful in the presence of a substantial degree of short-range order. Nevertheless, there seems every prospect of the fruitful inclusion of holographic crystallography, into the armory of techniques for atomic structure determination.

ACKNOWLEDGMENTS

We are grateful to J. Zhang and Z. L. Han for providing the measured diffraction pattern in Fig. 11. D.K.S. acknowledges support for this research by the donors of the Petroleum Research Fund, administered by the American Chemical Society, and by the Graduate School Research Committee of the University of Wisconsin–Milwaukee (UW-M). G.R.H. was supported in part by UW-M, and B.P.T. acknowledges a National Science Foundation Grant (No. DMR-88-05171).

[1]A. Szöke, in *Short Wavelength Coherent Radiation: Generation and Applications,* Proceedings of the Conference on Short Wavelength Coherent Radiation: Generation and Application, AIP Conf. Proc. No. 147, edited by D. J. Attwood and J. Boker (AIP, New York, 1986).
[2]J. J. Barton, Phys. Rev. Lett. **61**, 1356 (1988).
[3]D. K. Saldin and P. L. De Andres, Phys. Rev. Lett. **64**, 1270 (1990).
[4]D. Gabor, Nature (London) **161**, 777 (1948).
[5]G. R. Harp, D. K. Saldin, and B. P. Tonner, Phys. Rev. Lett. **65**, 1012 (1990).
[6]G. R. Harp, D. K. Saldin, and B. P. Tonner, Phys. Rev. B **42**, 9199 (1990).
[7]C. M. Wei, T. C. Zhao, and S. Y. Tong, Phys. Rev. Lett. **65**, 2278 (1990).
[8]C. M. Wei, T. C. Zhao, and S. Y. Tong, Phys. Rev. B **43**, 6354 (1990).
[9]B. P. Tonner, Z. L. Han, G. R. Harp, and D. K. Saldin, Phys. Rev. B **43**, 14 423 (1991).
[10]S. Y. Tong, C. M. Wei, T. C. Zhao, H. Huang, and Hua Li, Phys. Rev. Lett. **66**, 60 (1991).
[11]S. Hardcastle, Z.-L. Han, G. R. Harp, J. Zhang, B. L. Chen, D. K. Saldin, and B. P. Tonner, Surf. Sci. Lett. **245**, L190 (1991).
[12]D. K. Saldin and J. B. Pendry, Surf. Sci. **162**, 941 (1985).
[13]A. Liebsch, Phys. Rev. Lett. **32**, 1203 (1974).
[14]H. L. Davis and T. Kaplan, Solid State Commun. **19**, 595 (1976).
[15]S. Y. Tong, C. H. Li, and A. R. Lubinsky, Phys. Rev. Lett. **39**, 489 (1977).
[16]C. H. Li, A. R. Lubinsky, and S. Y. Tong, Phys. Rev. B **17**, 3128 (1978).
[17]J. B. Pendry, *Low Energy Electron Diffraction* (Academic, London, 1974).
[18]J. J. Barton and D. A. Shirley, Phys. Rev. B **32**, 1906 (1985).
[19]V. Fritzsche, J. Phys: Condens. Matter **2**, 1413 (1990); **2**, 9735 (1990).
[20]A. P. Kaduwela, D. Friedman, and C. S. Fadley (unpublished).
[21]J. J. Rehr and R. C. Albers, Phys. Rev. B **41**, 8139 (1990).
[22]P. J. Durham, J. B. Pendry, and C. H. Hodges, Comput. Phys. Commun. **29**, 193 (1982).
[23]D. D. Vvedensky, D. K. Saldin, and J. B. Pendry, Comput. Phys. Commun. **40**, 421 (1986).
[24]J. B. Pendry, in *Determination of Surface Structure by LEED,* edited by P. M. Marcus and F. Jona (Plenum, New York, 1984), p. 3.
[25]H. C. Poon and S. Y. Tong, Phys. Rev. B **30**, 6211 (1984).
[26]S. Y. Tong, H. C. Poon, and D. R. Snider, Phys. Rev. B **32**, 2096 (1986).
[27]H. Li and B. P. Tonner, Phys. Rev. B **37**, 3959 (1988).
[28]E. Hecht and A. Zajac, *Optics,* (Addison-Wesley, Reading, MA, 1980).
[29]R. J. Collier, C. B. Burckhardt, and L. H. Lin, *Optical Holography,* (Academic, New York, 1971).
[30]J. E. Kasper and S. A. Feller, *The Hologram Book* (Prentice-Hall, Englewood Cliffs, NJ, 1985).
[31]M. Born and E. Wolf, *Principles of Optics* (Pergamon, New York, 1959).
[32]Z.-L. Han, S. Hardcastle, G. R. Harp, H. Li, X.-D. Wang, J. Zhang, and B. P. Tonner, Surf. Sci. (to be published).
[33]See, e.g., M. M. Woolfson, *X-ray Crystallography* (Cambridge University Press, Cambridge, 1970).
[34]S. Thevuthasan, G. S. Herman, A. P. Kaduwela, R. S. Saiki, Y. J. Kim, and C. S. Fadley (unpublished).
[35]B. P. Tonner, Ultramicroscopy (to be published).
[36]J. J. Barton and L. J. Terminello, in *Structure of Surfaces-III,* edited by S. Y. Tong *et al.* (Springer-Verlag, Heidelberg, 1991).
[37]G. R. Harp, D. K. Saldin, X. Chen, Z. L. Han, and B. P. Tonner (unpublished).
[38]D. Gabor, Proc. Phys. Soc. **64**, 449 (1951).

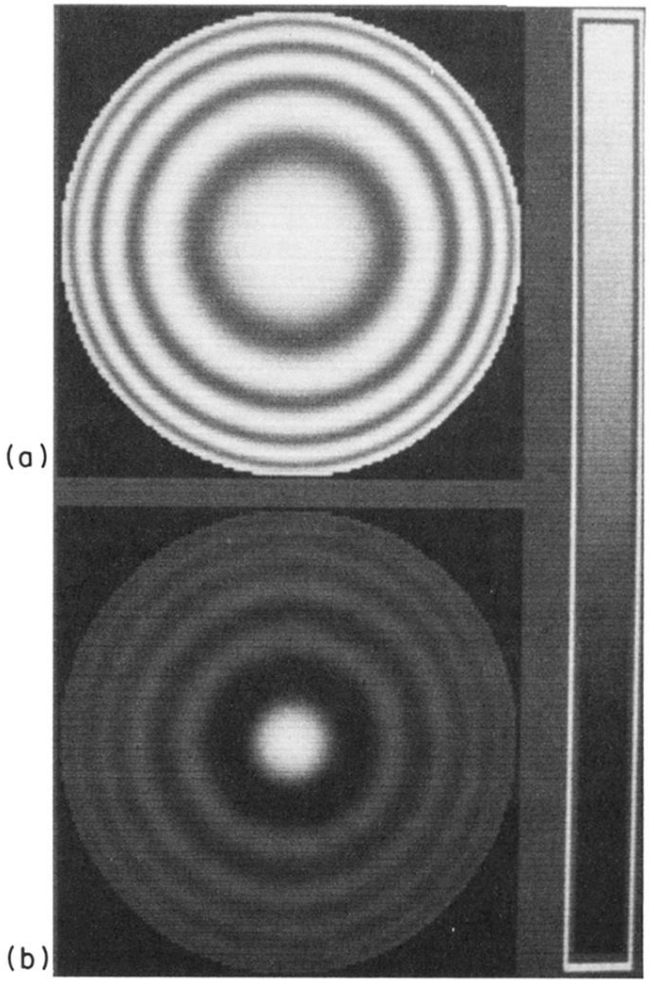

FIG. 1. (a) A Gabor zone plate, the forward-scattering Fraunhofer diffraction pattern generated by a point source of 914-eV electrons and an isotropic scatterer of zero phase shift 2.55 Å from the source. (b) An "atomic" zone plate from the same configuration as (a) but with the isotropic scatterer replaced by a Cu atom. In (b) a very prominent forward-scattering peak is observed with an extra fringe in the diffraction pattern.

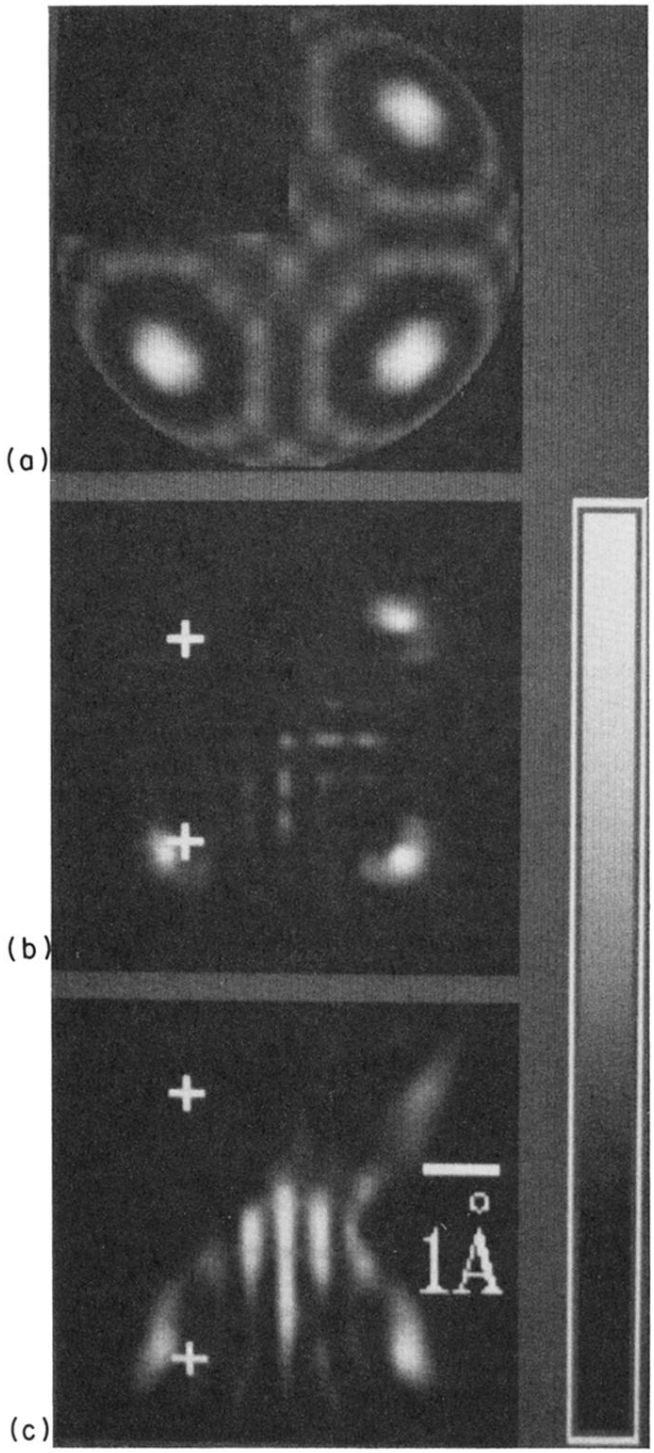

FIG. 10. (a) The diffraction pattern of Fig. 6, where we have blocked out one quarter of the data and (b) and (c) the same planar sections through the reconstructed image as in Fig. 6. We see the unexpected result that the atom *D* appears to be missing from the reconstruction. Forward scattering causes most of the measurable holographic fringes of an atom to be localized in a small part of the diffraction pattern. Thus, unlike optical holography, excising a part of a forward scattering hologram may remove specific features from its reconstruction.

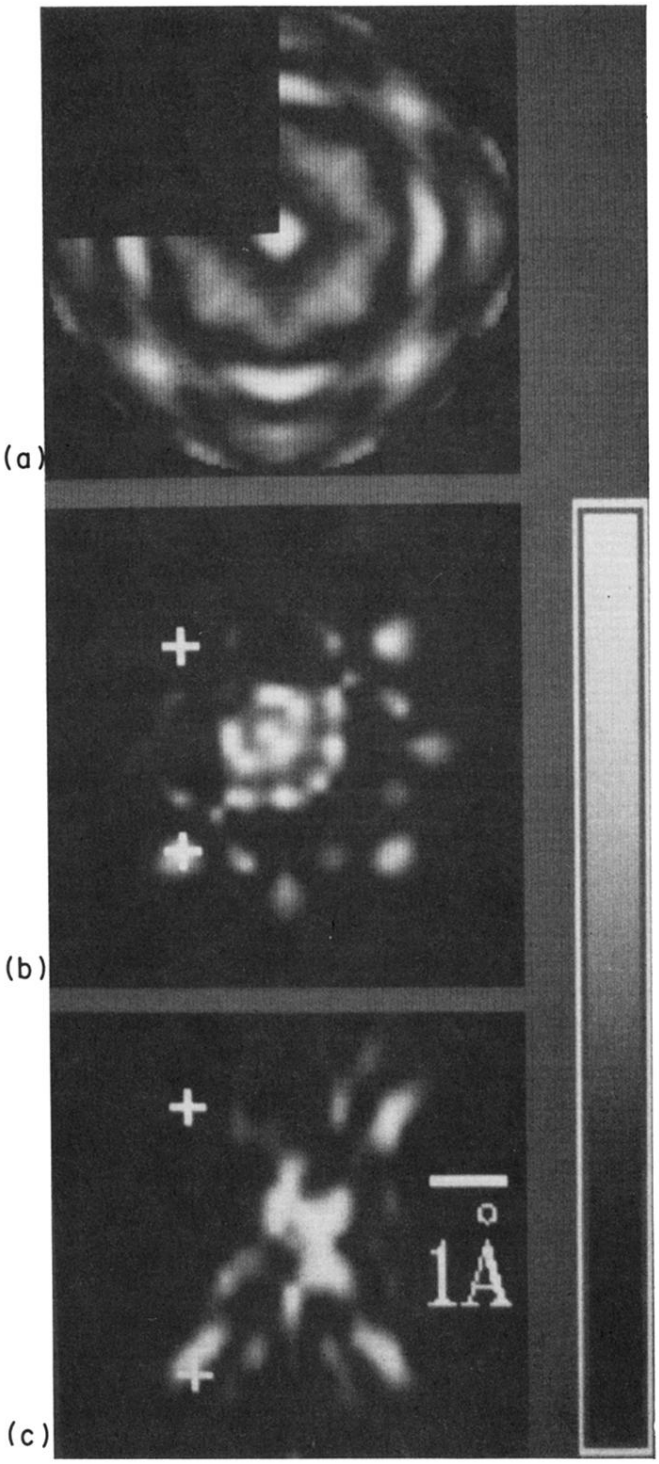

FIG. 11. We have performed the process of Fig. 10 on new Cu(100) single crystal Auger data to show this effect is reproduced using experimental data.

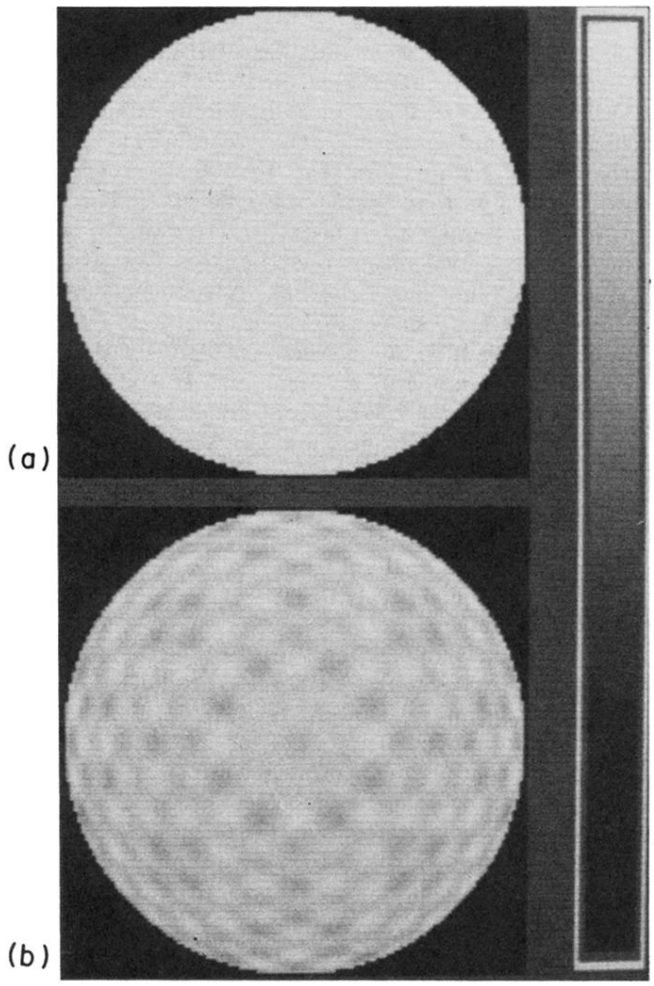

FIG. 12. Back-scattering diffraction patterns for a copper atom emitter with four copper atoms below it, at 300 K (a) and 100 K (b). The holographic fringes are practically immeasurable in (a) but may be measurable in (b), where the contrast is about 25% of that in Fig. 6(a).

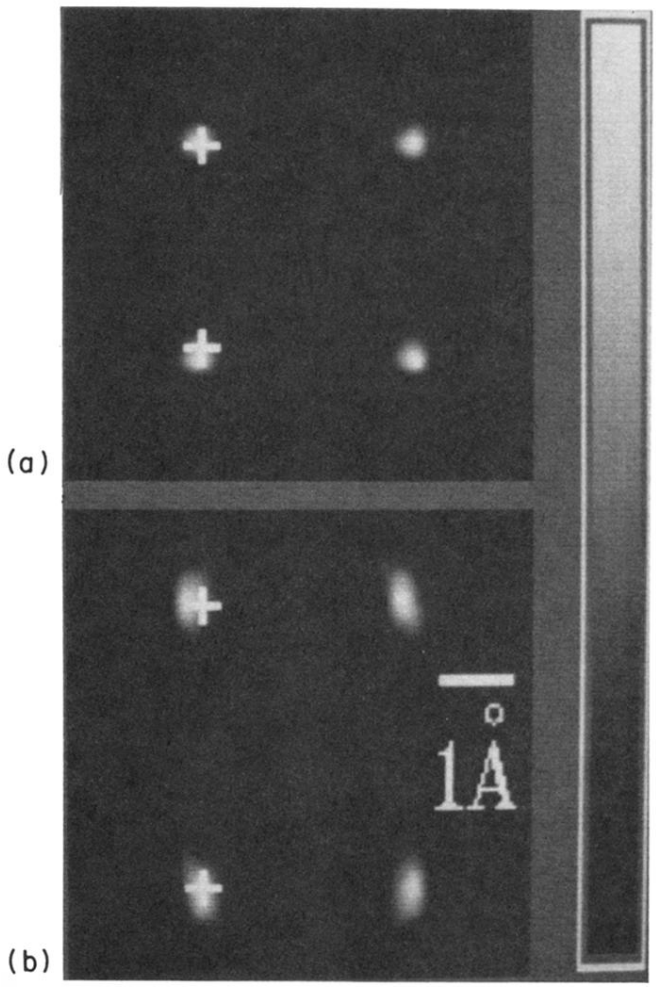

FIG. 13. The same sections through the reconstructed image from the diffraction pattern of Fig. 12(b) as in Fig. 5. Back-scattering patterns give sharp, artifact-free images, and this would be a desirable geometry for electron holography if the problems of the signal level could be overcome.

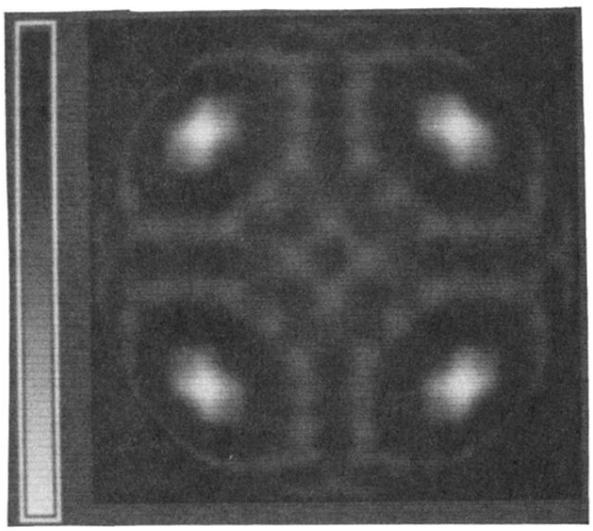

FIG. 14. The diffraction pattern from an emitter surrounded by all 12 of its nearest neighbors. This pattern is very similar to that of Fig. 6(a), showing that the four atoms that are situated between the emitter and the detector are the most important in determining the diffraction pattern.

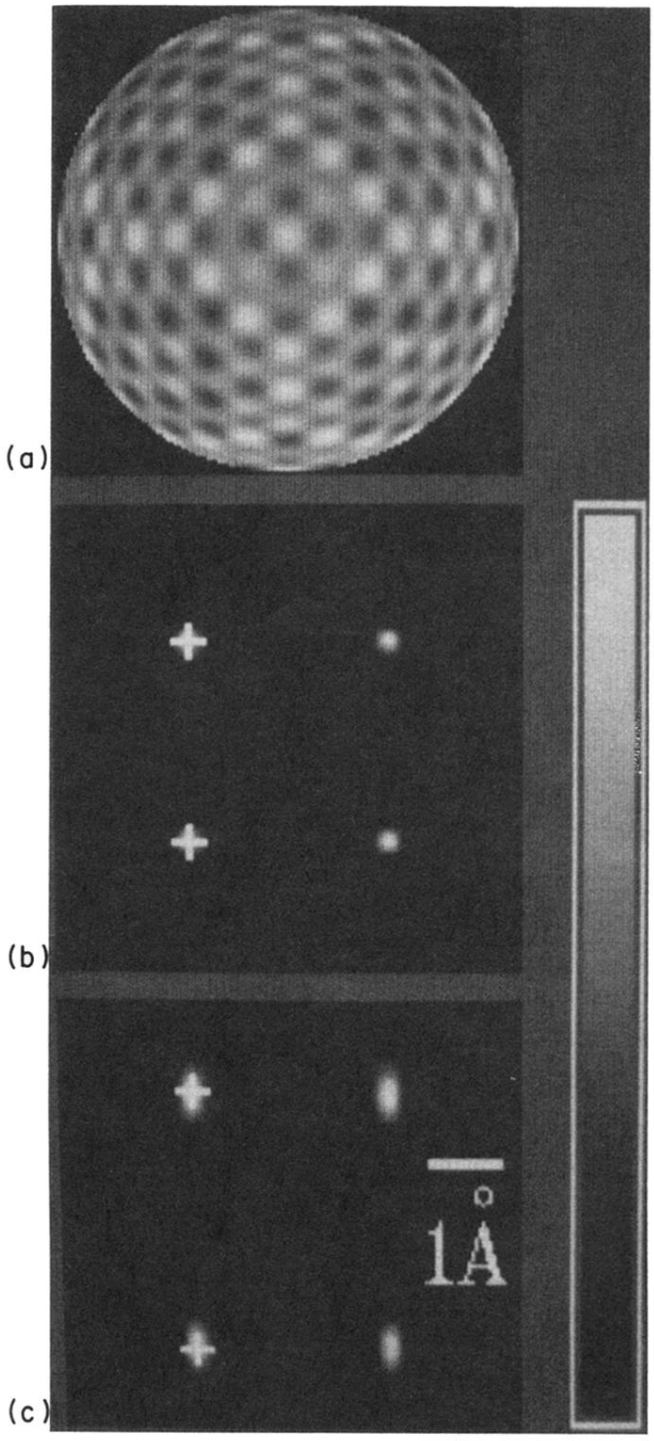

FIG. 5. (a) The diffraction pattern of four isotropic scatterers placed above the emitter. (b) and (c) contain sections of the reconstructed image from (a). Section (b) contains the four atoms *A*, *B*, *C*, and *D* of Fig. 4, and crosses mark the positions of atoms *A* and *D*. Section (c) contains the atoms *C* and *D*, and in the lower part of this section are the twin images of atoms *B* and *A*, which are found at the positions of atoms *E* and *F*. Crosses are placed at the positions of atoms *D* and *E*.

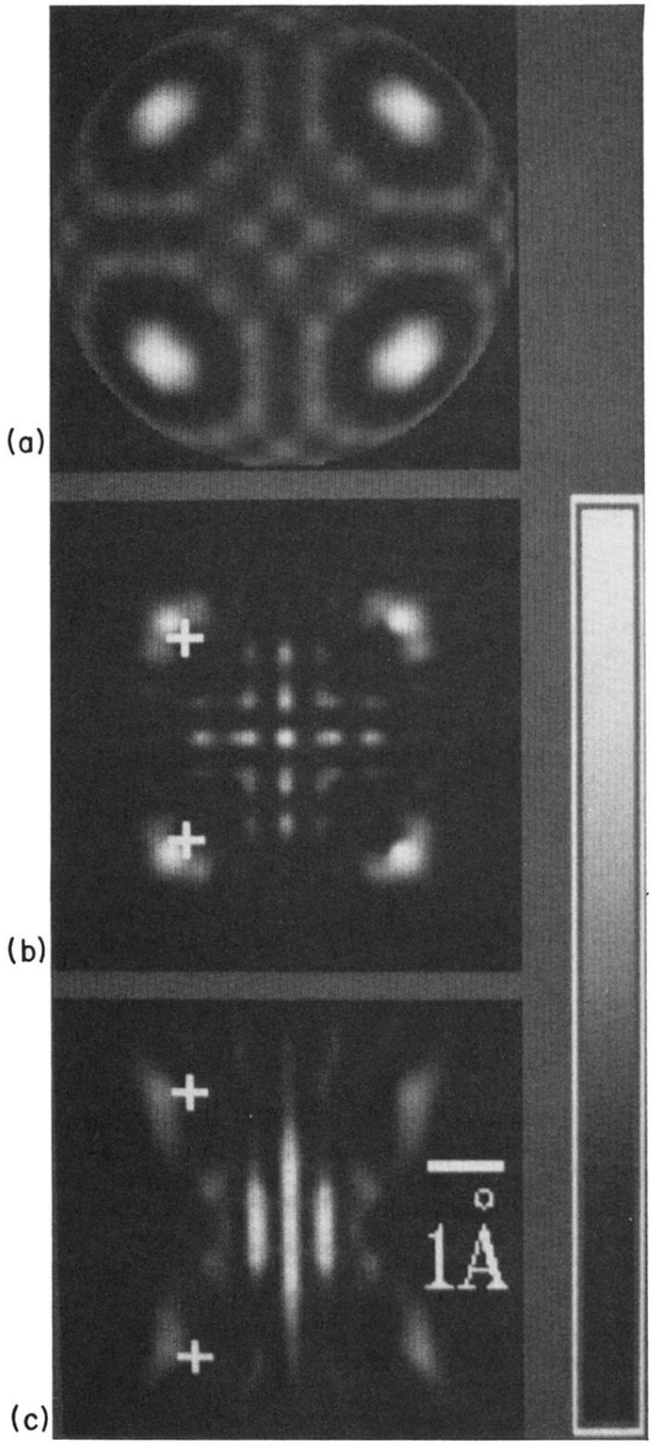

FIG. 6. The diffraction pattern and reconstructed images for copper atoms in the same geometry as for Fig. 5. The reconstructed images of the atoms appear distorted and shifted to larger distances from the emitter atom. Also seen are artifacts, away from atom positions, due to the forward-scattering features in the diffraction pattern.

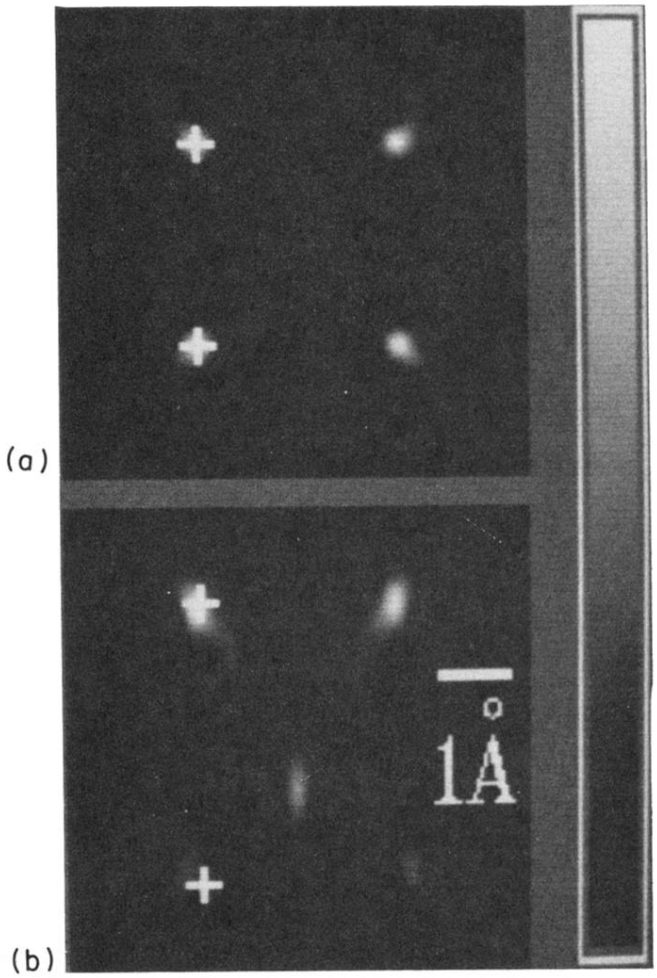

FIG. 8. The reconstructed intensity from the diffraction pattern of Fig. 6(a) in (a) the *ABCD* plane, and (b) the *CDEF* plane of Fig. 4 using the reconstruction scheme, which compensates for the phase of the atomic scattering factor. The images are shifted back to their true positions but still appear asymmetric.

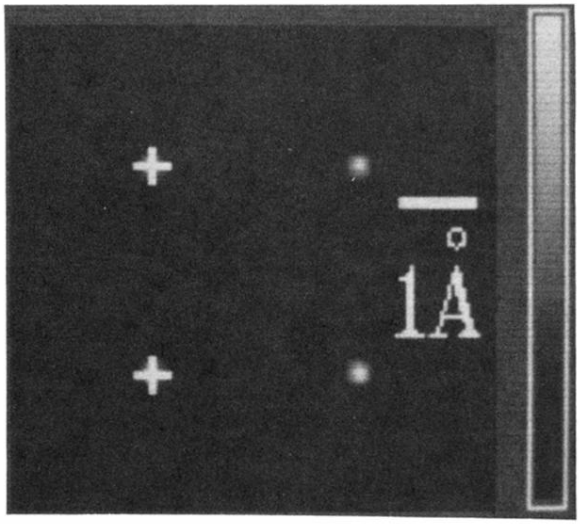

FIG. 9. Same as Fig. 8(a), but here using the reconstruction algorithm, which deconvolves the full atomic scattering factor from the image.